# Sex differences and risk factors for bleeding in Alagille syndrome

Simona Hankeova[1,2], Noemi Van Hul[1], Jakub Laznovsky[3], Katrin Mangold[1], Naomi Hensens[1,4], Elvira Verhoef[1,4], Tomas Zikmund[3], Feven Dawit[5], Michaela Kavkova[3], Jakub Salplachta[3], Marika Sjöqvist[1], Bengt R. Johansson[6], Mohamed Hassan[7], Linda Fredriksson[8], Vitezslav Bryja[2], Urban Lendahl[1], Andrew Jheon[7], Florian Alten[9], Kristina Teär Fahnehjelm[10], Björn Fischler[5], Jozef Kaiser[3] and Emma R. Andersson[1]*

## Affiliations

[1] Dept of Cell and Molecular Biology, Karolinska Institutet, Sweden.
[2] Dept of Experimental Biology, Masaryk University, Czech Republic.
[3] CEITEC – Central European Institute of Technology, Brno University of Technology, Czech Republic.
[4] University of Applied Sciences Utrecht, Netherlands.
[5] Dept of Pediatrics, Clinical Science, Intervention and Technology (CLINTEC), Karolinska Institutet and Karolinska University Hospital, Sweden.
[6] EM Unit, Institute of Biomedicine, University of Gothenburg, Sweden.
[7] University of San Francisco, United States of America.
[8] Dept of Medical Biochemistry and Biophysics, Karolinska Institutet, Sweden.
[9] Dept of Ophthalmology, University of Muenster Medical Center, Germany.
[10] Dept of Pediatric Ophthalmology, strabismus, electrophysiology and ocular oncology, St. Erik Eye Hospital, and Dept of Clinical Neuroscience, Karolinska Institutet, Stockholm, Sweden.
* Correspondence should be addressed to Emma R Andersson: emma.andersson@ki.se

## Abstract

**Spontaneous lethal bleeds are major cause of death in the pediatric liver disease Alagille syndrome (ALGS), yet risk factors and screening methods have not been established. We performed a systematic review and identified significantly more female than male patients with idiopathic intracranial hemorrhage (10:1). We investigated bleeding and vasculature in patients and a mouse model for ALGS (*Jag1*$^{Ndr/Ndr}$ mice) and asked whether phenotypes identified in mice could be detected in patients non-invasively. *Jag1*$^{Ndr/Ndr}$ mice bled spontaneously, exhibiting a thin skull and vascular defects including artery-vein crossings, tortuous vessels, capillary breakdown and CADASIL-like sparse vascular smooth muscle cell coverage which was aggravated by hypertension. Retinographs from patients confirmed tortuous blood vessels and artery-vein crossings in ALGS. In conclusion, *Jag1*$^{Ndr/Ndr}$ mice could be used to develop interventions for vascular defects in ALGS, and retinography could provide a non-invasive method for vascular analysis in these pediatric patients.**

## MAIN TEXT

### Introduction

Alagille syndrome (ALGS) is pediatric disorder characterized by liver and heart defects, as well as vertebral abnormalities, characteristic faces, and posterior embryotoxon (*1*, *2*). However, up to 25% of deaths in these patients are attributed to intracranial hemorrhage (*2–4*). Thus, in addition to the hallmark features, non-cardiac vascular stenosis, Moyamoya syndrome, vessel agenesis and spontaneous intracranial hemorrhage represent a significant burden of disease (*2*, *3*, *5*, *6*). Vascular defects are also a significant cause of transplant-associated complications (*3*). Bleeding can occur spontaneously, or upon minor head trauma, and is not correlated with liver-disease-induced coagulopathy (*7*). In some cases of minor head trauma leading to hemorrhage, cranial bone is described as inordinately thin (*6*, *8*), and is sometimes associated with "thin-walled arteries" (*6*, *8*, *9*). While these reports of bleeding in patients with ALGS show that vascular accidents can occur, it is not well understood which factors impact risk in patients, whether ALGS-like bleeding could be

modelled in mice, and whether vascular disease can be assessed non-invasively in this pediatric population.

ALGS is a genetic disorder caused by mutations in the Notch ligand *JAGGED1* or in the receptor *NOTCH2* (ALGS1; Online Mendelian Inheritance in Man/OMIM no. 118450, and ALGS2, OMIM no. 610205) (*10–12*). Notch signaling is a major blood vessel regulator, and Notch1/3/4 receptors, Delta like (Dll) 1/4 and Jagged1 (Jag1) ligands have key roles in endothelial cell (EC) growth, proliferation, arterial specification, and mural cell recruitment (*13–15*). Appropriate angiogenesis and vascular homeostasis are essential for organism health, and Notch pathway mutations are the cause of at least two congenital diseases with vascular involvement: Cerebral Autosomal Dominant Arteriopathy with Subcortical Infarcts and Leukoencephalopathy (CADASIL, mutations in *NOTCH3* (*16*)) and Adams Oliver syndrome (mutations in *NOTCH1*, *DLL4* or *RBPJk*, for review see (*17*)). It has been suggested that ALGS should also, in part, be considered a vascular disorder (*3*, *5*, *17*, *18*). The tight association of Notch mutations with congenital vascular diseases underscores the need for appropriate animal models of Notch-related disease, in which to test potential therapies. The recently reported *Jag1*$^{Ndr/Ndr}$ mouse model for Alagille syndrome recapitulates cholestatic liver disease in postnatal pups (*19*) with spontaneous liver regeneration in adults (*20*), as well as cardiac phenotypes and ocular anomalies (*19*). This mouse model could thus provide an important model for preclinical studies, if it also recapitulates bleeding, reported risk factors, or vascular anomalies present in patients.

Understanding vascular events in ALGS is complicated by the roles of Notch in vascular development, and the multiple possible risk factors in ALGS for bleeding, from frail bones (*21*) to coagulopathy as a consequence of liver disease. Although coagulation factors are dysregulated in liver disease, "re-balancing" of pro- and anti-coagulant activity is thought to leave patients in a balanced but fragile coagulant state (*22*), and it is not well understood whether liver disease in ALGS functionally impacts on bleeding. Furthermore, different types of bleeds in ALGS may have different etiologies, from gastrointestinal bleeds due to espohageal varices and portal hypertension, to ruptured intracranial aneurysms. In the general population, more men are reported with cirrhosis and bleeding due to esophageal varices (*23*) and men have a 60% greater risk of intraberebral hemorrhage (*24*). However, subarachnoid hemorrhage is more prevalent in women than men after age 55 (*25*). It would thus be expected that sex could impact the prevalence of various types of bleeds in ALGS.

To comprehensively analyse vascular disease in patients with ALGS we first performed a systematic review of the literature, extracting all patients with sex data and vascular anomalies or bleeding events. To understand mechanisms of intracranial bleeding, we investigated spontaneous bleeding and risk factors including coagulopathy and skull bone thickness, as well as angiogenesis, hypertension and vascular homeostasis in male and female *Jag1*$^{Ndr/Ndr}$ mice. Finally, we asked whether vascular anomalies discovered in the mouse model could be identified and quantified non-invasively in retinographs from pediatric patients with ALGS. First, the systematic review identified an increased prevalence of idiopathic intracranial hemorrhages in female patients with ALGS (10:1). Secondly, *Jag1*$^{Ndr/Ndr}$ mice displayed spontaneous bleeds in multiple organs, in the absence of coagulopathy, and exhibited a thin skull and multiple angiogenic and vascular homeostatic defects. Finally, vascular anomalies discovered in the mouse model could be identified and quantified in retinographs from pediatric patients, providing a method for non-invasive investigation of vascular health in ALGS. In sum, we show that multiple risk factors are present to predispose patients with ALGS to potentially lethal intracranial bleeds. The *Jag1*$^{Ndr/Ndr}$ mouse which recapitulates spontaneous bleeds and multiple risk factors, could provide an important pre-clinical model to investigate and test therapeutic approaches.

## Results

*Patients with Alagille syndrome exhibit sporadic spontaneous and provoked hemorrhages, with sex-differences*

Previous studies have shown that vascular defects are common in ALGS, but have not reported any sex differences in vascular defects in general (*3*, *9*, *26*) or in prevalence of intracranial bleeds, a major cause of death (*2–4*). We therefore first asked which vascular events were most often reported in patients, and whether vascular events were affected by sex, focusing on intracranial events. ALGS is a rare disorder, and assembling large cohorts is therefore a major challenge. In order to methodically map vascular defects in the largest possible group of patients with vascular events, we performed a systematic literature review adhering to the Prisma guidelines (*27*), and assessed the full text of 771 publications. Cardiac-associated defects (including pulmonary stenosis) and esophageal varices (expected to be secondary to portal hypertension) were excluded from analysis in order to identify primary vascular defects. We identified 172 patients with ALGS, sex data available, and vascular defects including vascular structural abnormalities or vascular events (Fig. 1A, Fig. S1, Table S1, for search terms and strategy see Materials and Methods). The most frequently reported structural abnormalities were stenoses, collateral vessels/occlusions and aneurysms (Fig. S1A, Table S1). There were no sex differences in the reported structural anomalies. The most frequently reported functional events were bleeding events, surgery-related vascular complications and ischemic events (Fig. S1B, Table S1). Among the bleeding events, the predominantly reported type was intracranial bleeding followed by pulmonary hemorrhage (Fig.1B, Table S1). Other rare bleeding events included nasal, ocular, pancreatic, or post liver biopsy bleeding and hematemesis (Table S1). There were no sex differences in ischemic events, surgery-related vascular complications,

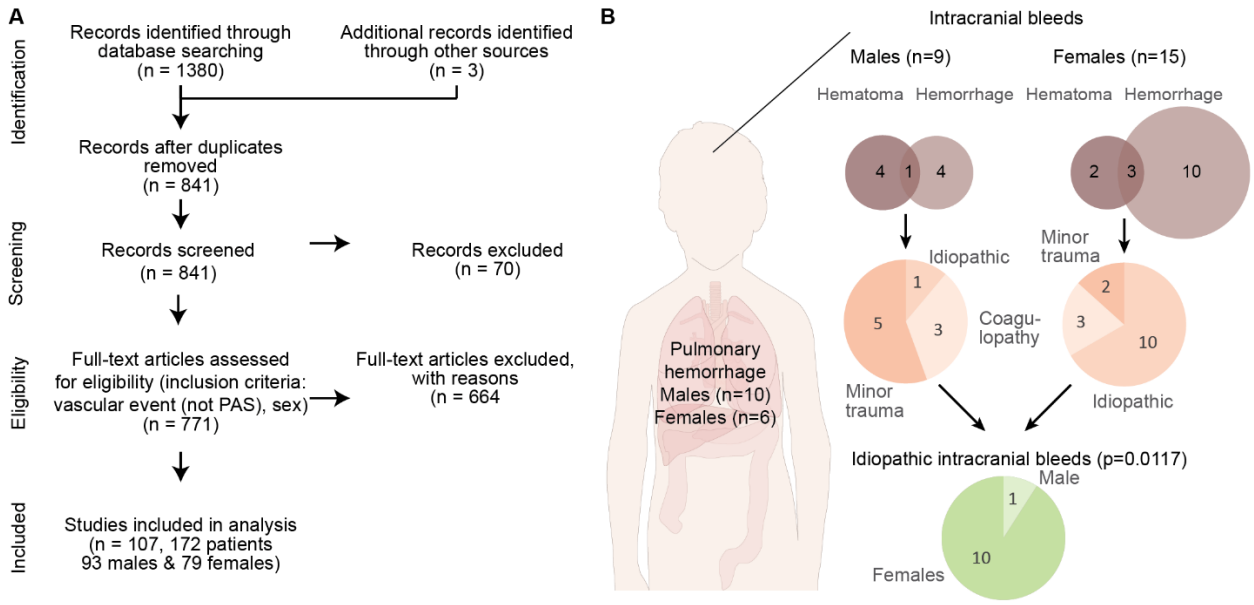


Fig. 1. **Patients with Alagille syndrome exhibit sporadic spontaneous and provoked hemorrhages, with sex-differences. (A)** Systematic review search strategy that identified 107 relevant publications describing 172 individuals with Alagille syndrome (ALGS) and vascular events (excluding pulmonary artery stenosis) including sex data. **(B)** Schematic depicting the most frequently reported bleeding events in patients with ALGS, pulmonary hemorrhage (n=16, Binominal test for equal prevalence in 10 males vs 6 females, ns, P=0.3323) and intracranial bleeds (n=24, Binominal test for equal prevalence in 9 males vs 15 females, ns, P=0.2295). Intracranial bleeds were the result of either hematoma (males n=5, females n=5, Binomial test for equal prevalence ns P >0.9999) or hemorrhage (males n=5, females n=13, Binomial test for equal prevalence ns P=0.0963). The underlying causes of the intracranial bleeds were either minor head trauma or coagulopathy, or they were idiopathic (pie charts denote reported patient numbers). Pie chart depicting the number of idiopathic intracranial bleeds (male n=1, females n=10, Binominal test for equal prevalence, *P=0.0117). For details of intracranial bleeds and references, please see Table 1. ALGS, Alagille syndrome; PAS, pulmonary artery stenosis.

overall bleeding events, or in pulmonary hemorrhages (Fig. 1B, Fig. S1B).

Intracranial bleeds included: six patients with brain hematomas (two females and four males), fourteen patients with brain hemorrhages (ten females and four males) and four patients with both (three females and one male) (Fig. 1B, Table 1). Intracranial bleeds were the result of either minor head trauma often associated with a paper-thin skull, coagulopathy induced by liver cholestasis, or were idiopathic (Fig. 1B, Table 1, Table S1). Patients with minor head trauma or coagulopathy exhibited intracranial bleeding at a young age, on average 5.9 years for males and 8.3 years for females, and there were no sex differences in this group (Table 1). In contrast, idiopathic brain hemorrhages were typically the consequence of a ruptured aneurysm and happened at later ages, specifically at thirteen years for the one male and on average 16.5 years in females (age range 4-30 years old). There were significantly more idiopathic brain hemorrhages in females than males (10 vs 1, Fig. 1B, Table 1, Table S1, two-sided binominal exact test P=0.0117).

In sum, this analysis systematically aggregates all available bleeding and vascular data for patients with Alagille syndrome, and shows that female sex is a risk factor for idiopathic brain hemorrhage caused by a ruptured aneurysm (Fig. 1B, Table 1, Table S1).

### *Cholestatic Jag1$^{Ndr/Ndr}$ mice exhibit normal coagulation but a thinner skull and sporadic spontaneous and provoked hemorrhages*

To investigate mechanisms contributing to bleeds, and whether the recently reported *Jag1*$^{Ndr/Ndr}$ mouse model for ALGS recapitulates risk factors reported in patients, we analyzed known factors associated with bleeding events in cholestasis in general or ALGS specifically, including coagulopathy and thin/fragile intracranial bones, respectively. Sixteen *Jag1*$^{Ndr/Ndr}$ pups were monitored during the first 10 days after birth. One of the sixteen *Jag1*$^{Ndr/Ndr}$ pups died with a macroscopic brain bleed (one of the 2/53 also reported further below), and six *Jag1*$^{Ndr/Ndr}$ pups were lost to analysis (deaths = 7/16, 43.8%, Fig. 2A). The *Jag1*$^{Ndr/Ndr}$ pups died between P1 – P6, and were cannibalized by the mothers, preventing further analysis (Fig. 2A). At P10, surviving *Jag1*$^{Ndr/Ndr}$ pups were jaundiced and total bilirubin was significantly increased (Fig. 2B and (*19*)). Despite cholestastis, coagulation activity was normal at P10, as demonstrated by normal levels of Thrombin-Antithrombin (TAT) complexes in blood plasma (Fig. 2C), fibrinogen in serum (Fig. 2D), INR in complete blood (Fig. 2E) and tail bleeding time (Fig. 2F). Qualitative analysis of *Jag1*$^{Ndr/Ndr}$ skulls using micro computed tomography (μCT) revealed craniosynostosis in 4 of 6 *Jag1*$^{Ndr/Ndr}$ mice examined (Fig. 2G, green arrowheads), which is also found in patients with ALGS (*2*, *26*, *28*). *Jag1*$^{Ndr/Ndr}$ cranial bones were thinner than in wild type mice, and often consisted of a single layer of compact bone, rather than two layers of compact bone (Fig. 2G right panels) encasing the spongy bone and trabeculae (Fig. 2G middle panels, compare the solid color in the middle panel in wild type mice (full thickness width, with corresponding cross-section at right) to the speckled pattern in the right panel (shortest distance width = top layer of compact bone separated from bottom layer by trabeculae, notable in corresponding cross-section at right)). In contrast, *Jag1*$^{Ndr/Ndr}$ parietal bone had similar widths in the whole width and the shortest width/compact bone analyses. *Jag1*$^{Ndr/Ndr}$ pups are strikingly smaller than wild type animals (*19*) and, accordingly, the *Jag1*$^{Ndr/Ndr}$ adult skull lengths were smaller in size than wild types and were, on average, 91.8% of the wild type skull lengths (Fig. S2A, P=0.003). However, the volume of the *Jag1*$^{Ndr/Ndr}$ cranial bone full width (Fig. 2H, ~ 76% of wild type volume) and the compact bone (Fig. 2I, ~ 76% of wild type volume) were both disproportionately and significantly lower than wild type skull volumes. The greater decrease in the cranial bone volume compared to length (76 vs 91%), and the bone fusion seen in parietal bone (Fig. 2G) thus demonstrate a thinner skull in *Jag1*$^{Ndr/Ndr}$ mice.

To test bleeding and blood vessel permeability in the kidney, heart and liver, we used the Evans blue assay. There was a mild, non-statistically significant, increase in kidney vessel permeability in adult *Jag1*$^{Ndr/Ndr}$ mice

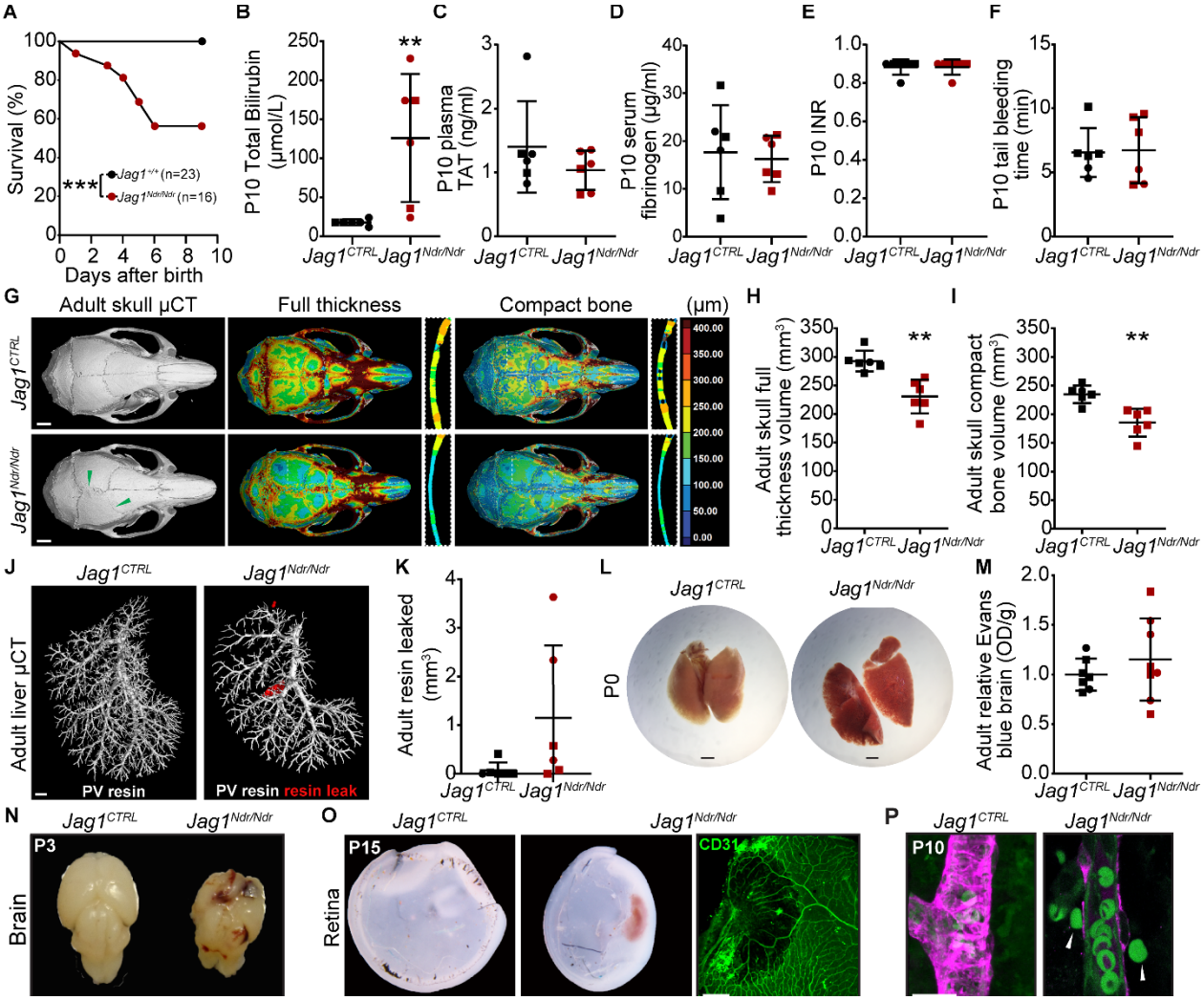


Fig. 2. **Cholestatic *Jag1*$^{Ndr/Ndr}$ mice exhibit normal coagulation but a thinner skull and sporadic spontaneous and provoked hemorrhages.** (A) Pup survival analysis between P0 and P10. Each dot represents the absolute percent of remaining animals in the group (Long-rank test, ***P=0.0006). (B) Total bilirubin levels in plasma at P10 (n=6 per condition, Unpaired t test, **P=0.0091). (C) Thrombin Antithrombin (TAT) enzyme-linked immunosorbent assay (ELISA) from plasma of postnatal day 10 (P10) mice (n=6 per condition, Unpaired t test, ns, P=0.2788). (C) Fibrinogen ELISA of serum from P10 mice (n=6 per condition, Unpaired t test, ns, P=0.7585). (E) Prothrombin time (INR) of whole blood from P10 mice (n=6 per condition, Unpaired t test, ns, P>0.9999). (F) Tail bleeding time in P10 mice (n=6 per condition, Unpaired t test, ns, P=0.8916). (G) Micro computed tomography (µCT) of adult skulls (left panel), the green arrowheads denote fused sutures in *Jag1*$^{Ndr/Ndr}$ mice. Color map depicting wall thickness of periosteum. Dotted lines denote the section planes in middle panels. Color map depicting wall thickness of compact bone, including trabeculae (diploë). Dotted lines denote the section plane, in right panels, in which diploë were excluded (black spaces in bone). Scale bar 2 mm. (H) Total volume of skull (based on wall thickness analysis) (n=6 per condition, Unpaired t test, **P=0.0014) (I) Total volume of intracranial compact bone (excluding diploë, based on wall thickness analysis) (n=6 per condition, Unpaired t test, **P=0.0017). (J) Resin injection into the portal vein followed by (K) quantification of resin leakage outside of the blood vessels (in red) in adult mice (*Jag1*$^{CTRL}$ n=7, *Jag1*$^{Ndr/Ndr}$ n=8, Unpaired t test, ns, P=0.1088). Scale bar 1 mm. (L) Lung hemorrhages in *Jag1*$^{Ndr/Ndr}$ P0 pups (n=6 mice of which 4 males and 2 females, bleeds present in 2 males). Scale bar 1 mm. (M) Blood brain barrier permeability tested by Evans blue assay of the adult brain parenchyma (n=6 per condition, Unpaired t test, ns, P=0.3807). (N) Brain from P3 *Jag1*$^{Ndr/Ndr}$ pup, which died due to brain hemorrhages (n= 2 of 53 *Jag1*$^{Ndr/Ndr}$ mice, sex n.d.). (O) P15 *Jag1*$^{Ndr/Ndr}$ mouse with spontaneous retinal bleeding. Scale bar 20 µm. Sex n.d. (P) Red blood cells present outside the arterial vessel wall in P10 *Jag1*$^{Ndr/Ndr}$ retina. Scale bar 5 µm. Graphs lines depict mean values ± standard deviation. Circles represent females, squares represent males. µCT, micro computed tomography; n.d., not determined; OD, optical density; TAT, Thrombin Antithrombin; P(X), postnatal day X; P = , calculated probability.

(P=0.0671, Fig. S2B), in which three of eight *Jag1*$^{Ndr/Ndr}$ mice displayed higher Evans blue values in kidney than the highest wild type values. Evans blue values were similar for wild type and *Jag1*$^{Ndr/Ndr}$ mice in heart and liver (Fig. S2C, S2D). We measured blood vessel fragility and risk of provoked bleeds by analyzing resin leakage from synthetic resin injections intthe hepatic portal vein (*20*). Two of six *Jag1*$^{Ndr/Ndr}$ mice (both females) had 40x more resin outside of the portal vein than the average of control animals, with macroscopically obvious leakage (leaks pseudo colored red, Fig. 2J, 2K).

In order to investigate spontaneous vascular accidents we next examined the lungs, brain and the retina. There were lung hemorrhages in two of six P0 *Jag1*$^{Ndr/Ndr}$ mice (group = 4 males and two females, bleeds in 2 males) while none were observed in wild type pups (0/6 examined) (Fig. 2L). To test blood brain barrier integrity we analyzed Evans blue-injected adult brains. Three adult *Jag1*$^{Ndr/Ndr}$ mice (one male, two females) of eight tested, had mildly increased Evan blue leakage in the brain compared to the wild type animals, but on average there was no difference (Fig. 2M). Fifty-three *Jag1*$^{Ndr/Ndr}$ pups were monitored daily from birth until P10 and macroscopically obvious brain hemorrhages occurred in two *Jag1*$^{Ndr/Ndr}$ pups (3.77%) but were not observed in wild type or heterozygous mice (Fig. 2N, Fig. S2G, blue arrowheads indicate bleeds in head region, sex n.d.). In surviving pups at P10 and P15, *Jag1*$^{Ndr/Ndr}$ pups also sporadically displayed retinal hemorrhage (Fig. 2O, sex n.d.) or leaky retinal arterioles (Fig. 2P, sex n.d.).

In summary, our data show that 3 – 4% of *Jag1*$^{Ndr/Ndr}$ mice exhibit spontaneous central nervous system bleeds. *Jag1*$^{Ndr/Ndr}$ mice thus recapitulate spontaneous and rare bleeds in different organs, in the absence of detectable coagulation defects. Similar to patients with ALGS, thinner skulls in *Jag1*$^{Ndr/Ndr}$ mice are likely to contribute to nervous system bleeds.

### *Delayed retinal vascular outgrowth and remodeling in Jag1*$^{Ndr/Ndr}$ *mice*

JAG1 is a proangiogenic ligand balancing the number of tip cells and stalk cells (*13*). We therefore investigated retinal sprouting angiogenesis in the mouse model for ALGS. The retina is part of the central nervous system and is vascularized postnatally in mice: during the first fifteen days after birth three capillary plexuses are established in the tissue (schematic Fig. 3A, S – superficial, I – intermediate and D – deep capillary plexus) (*29*). At P5, retinal blood vessels in *Jag1*$^{Ndr/Ndr}$ mice were significantly delayed in outgrowth, a defect that was not symmetric between left and right eyes (Fig. 3B, 3C). The delayed extension and growth persisted throughout angiogenesis, marked by delayed vertical sprouting to the deep capillary plexus at P10 (Fig. S3A), and reduced extension of the intermediate capillary plexus at P15 (Fig. S3B, green capillary bed). The number of tip cells was mildly but not significantly decreased at the vascular front at P5 (Fig. 3D left panels, Fig. 3E), but tip cells displayed an increase in tips per tip cell, with filopodia extending in several directions per cell (Fig. 3D blue arrowheads in right panels, Fig. 3F). The overall number of filopodia per tip or tip cell was similar in wild type and *Jag1*$^{Ndr/Ndr}$ mice (Fig. S3C).

We analyzed vascular plexus remodeling during angiogenesis at P5, P10 and P15 (Fig. 3G – 3M), and total vascular length per field was significantly shorter at P5, comparable at P10, and significantly increased at P15, in *Jag1*$^{Ndr/Ndr}$ retinas (Fig. 3G – 3J), indicating both delayed outgrowth and reduced remodeling. The total vascular length reflected differences in EC numbers, as evidenced by a significant decrease in ERG+ ECs at P5 and a significant increase at P15 in *Jag1*$^{Ndr/Ndr}$ mice (Fig. 3G – 3J, 3K). The number of ECs normalized to vascular length was similar between *Jag1*$^{Ndr/Ndr}$ and wild type mice (Fig. 3L), indicating the delayed outgrowth (Fig. 3B, 3C) is not due to migratory defects. The number of branching points was significantly lower at P5 in *Jag1*$^{Ndr/Ndr}$ retinas but similar at P10 and P15 (Fig. 3G – 3I, 3M). To determine whether the differences in blood vessel outgrowth were a consequence of altered proliferation, we quantified the number of phosphorylated histone 3 (PH3) and Pecam1 (CD31) double positive cells per area, in 200 µm long zones (in total 12 zones) from the optic

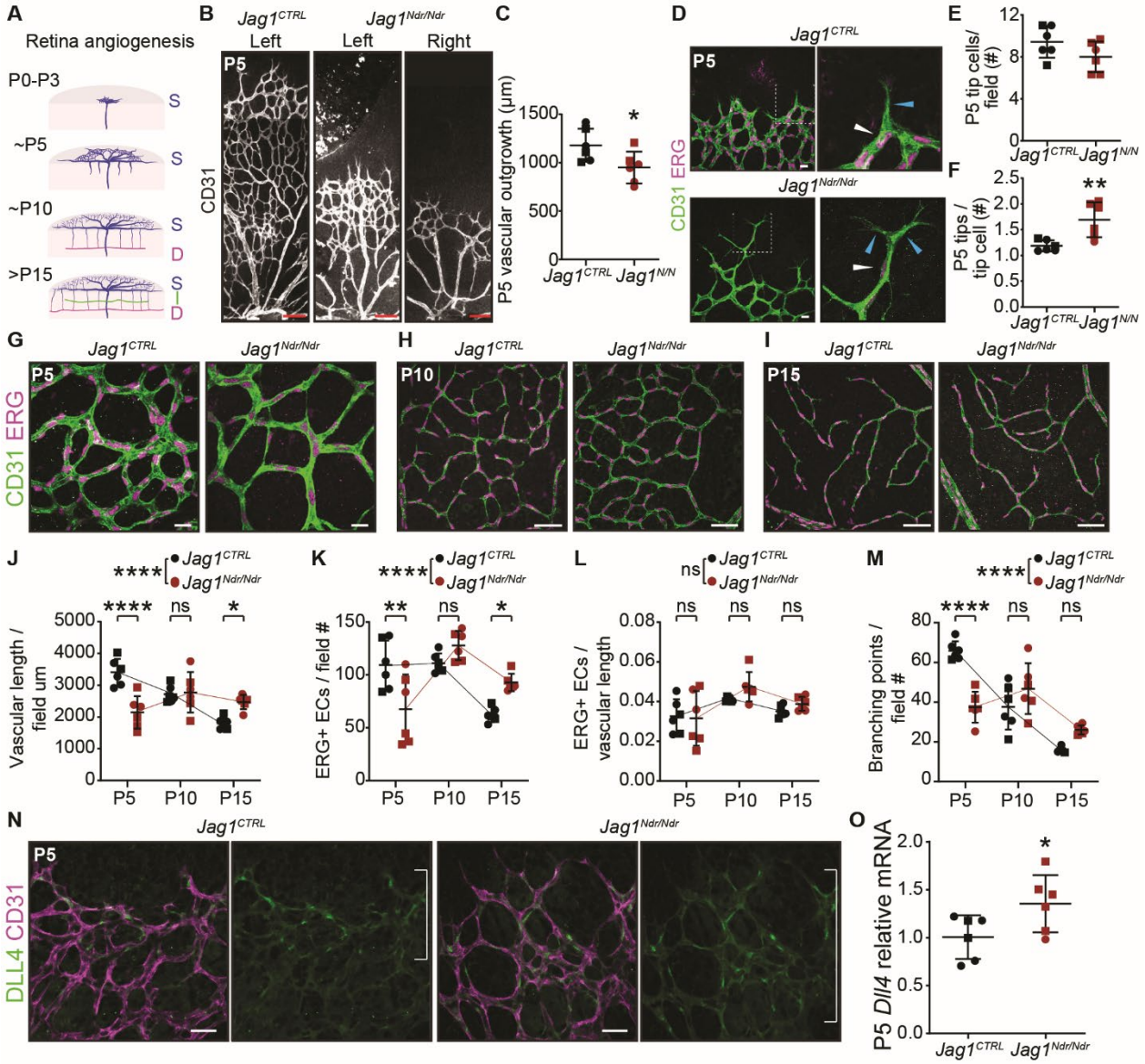


Fig. 3. **Delayed retinal vascular outgrowth and remodeling in *Jag1*$^{Ndr/Ndr}$ mice. (A)** Schematic depicting retinal angiogenesis between postnatal day 0 (P0) and P15. During the first 15 days after birth, three capillary plexuses are established S – superficial, I – intermediate, D – deep capillary plexus. **(B)** *Jag1*$^{Ndr/Ndr}$ retinal vasculature stained for CD31 (Pecam1) was delayed in outgrowth, quantified in **(C)** (n=6 per condition, Unpaired t test, *P=0.0388). Scale bar 100 µm. **(D)** Immunofluorescence staining of P5 vascular front with endothelial tip cells (boxed region). White arrowhead points to ERG+ nucleus of a tip cell, quantified in **(E)** (n=6 per condition, Unpaired t test, ns, P=0.1281). Blue arrowheads point to tips (bundles of filopodia) of tip cells quantified in **(F)** (n=6 per condition, Unpaired t test, **P=0.0059). Scale bar 20 µm. **(G-I)** Retinal vasculature at (G) postnatal day 5 (P5), **(H)** P10 and **(I)** P15. Scale bars 20 µm (G), 50 µm (H, I). **(J – M)** Quantification across retinal blood vessel development at P5, P10 and P15 of **(J)** vascular length per field (n=6 per condition, Two-way ANOVA interaction, ****P<0.0001, Sidak's multiple comparisons test P5 ****P<0.0001, P10 ns, P=0.9927, P15 *P=0.0233). **(K)** Number of endothelial cells (ERG+) per field (n=6 per condition, Two-way ANOVA interaction, ****P<0.0001, Sidak's multiple comparisons test P5 **P=0.0013, P10 ns, P=0.3204, P15 *P=0.0217). **(L)** Number of endothelial cells (ERG+) per vascular length (n=6 per condition, Two-way ANOVA interaction, ns, P=0.4617, Sidak's multiple comparisons test P5, ns, P=0.9938, P10 ns, P=0.3560, P15, ns, P=0.7820). **(M)** Number of branching points per field (n=6 per condition, Two-way ANOVA interaction, ****P<0.0001, Sidak's multiple comparisons test P5 ****P<0.0001, P10 ns, P=0.1560, P15, ns, P=0.0979). **(N)** Delta like 4 (DLL4) immunofluorescence in the vascular front at P5. Scale bar 20 µm. White brackets denote area with high DLL4 intensity. **(O)** *Dll4* relative mRNA levels in whole retina lysates (n=6 per condition, Unpaired t test, *P=0.0461). Each dot represents quantification from one animal; graphs depict mean values ± standard deviation. Circles represent females, squares represent males. D, deep capillary plexus; I, intermediate capillary plexus; P(X), postnatal day X; P = , calculated probability; S, superficial capillary plexus.

nerve (Fig. S3D, scheme). The bell-shaped proliferation curve peak was in Zone 4 (800 µm from the optic nerve) in *Jag1*$^{Ndr/Ndr}$ mice, while the peak was in Zone 5 (1,000 µm from the optic nerve) in wild type mice (Fig. S3E). At P10 and P15 the number of proliferating ECs was lower in both *Jag1*$^{Ndr/Ndr}$ and wild type retinas, and their distribution was similar (Fig. S3F, S3G). At P15, the *Jag1*$^{Ndr/Ndr}$ vascular front had reached the retina periphery (Fig. S3G).

JAG1 competes with the ligand DLL4 for the NOTCH1 receptor and loss of JAG1 leads to upregulation of DLL4 (*13*). Analysis of Dll4 expression revealed that DLL4 protein expression was highest in the vascular front and in tips cells in *Jag1*$^{CTRL}$ mice while it was more widespread in the *Jag1*$^{Ndr/Ndr}$ vascular front (Fig. 3N, white brackets) and *Dll4* mRNA levels in *Jag1*$^{Ndr/Ndr}$ whole retina lysates were significantly increased (Fig. 3O). To test whether neutralizing DLL4 would normalize the vasculature in *Jag1*$^{Ndr/Ndr}$ mice, we injected pups with a DLL4-neutralizing antibody (aDLL4) (*30*) at P2, and analyzed retinas 48 hours later. As reported previously (*31*), treatment with aDLL4 (0.0025 mg/g) did not affect vascular outgrowth in wild type mice, (Fig. S3H, S3I), but did significantly increase vascular density, with an increased number of branching points in wild type mice. However, aDLL4 did not rescue outgrowth or branching in *Jag1*$^{Ndr/Ndr}$ pups (Fig. S3H, S3J).

Taken together, our results confirm that JAG1 is necessary for blood vessel outgrowth, branching, remodeling and proliferation, as reported previously for the EC-specific *Jag1* knockout (*13*). Although DLL4 was increased at the RNA level and was more widespread in *Jag1*$^{Ndr/Ndr}$ retina, blocking DLL4 was not sufficient to rescue the vascular defects in *Jag1*$^{Ndr/Ndr}$ mice. Our analysis further revealed that, in *Jag1*$^{Ndr/Ndr}$ retinas, tip cells are not significantly reduced in number, but they form hyperbranched elongated tips. Finally, despite the delay in proliferation and outgrowth at P5, the *Jag1*$^{Ndr/Ndr}$ superficial vasculature plexus was normalized by P15.

### *Jag1*$^{Ndr/Ndr}$ *mice display vascular guidance defects, with fewer and more tortuous blood vessels*

Abnormal blood vessel growth or patterning can cause changes in blood flow leading to vessel occlusion (*32*), changes in shear stress (*33*) and changes to the vessel wall that result in blood vessel tortuosity/dolichoectasia associated with vascular lesions and stroke (*34*). We analyzed the presence of arteriovenous crossings, which are considered pathological in mouse retina (*35*), and found an average of two arteriole/venule crossings per *Jag1*$^{Ndr/Ndr}$ retina in both males and females (Fig. 4A, 4B). *Jag1*$^{Ndr/Ndr}$ males and females had significantly fewer arterioles (Fig. 4C) compared to same sex *Jag1*$^{CTRL}$ mice and *Jag1*$^{Ndr/Ndr}$ females had fewer venules compared to *Jag1*$^{Ndr/Ndr}$ males and *Jag1*$^{CTRL}$ females (Fig. 4D). Arterial tortuosity was increased in three of six *Jag1*$^{Ndr/Ndr}$ mice at P30 (Fig 4E) and in one of six *Jag1*$^{Ndr/Ndr}$ mice at one year (Fig 4F), but the overall differences were not statistically significant. In contrast, overall venous tortuosity was significantly increased in *Jag1*$^{Ndr/Ndr}$ mice independent of age (Fig 4G, 4H), an effect that was driven by increased tortuosity in female *Jag1*$^{Ndr/Ndr}$ mice at P30 (one way ANOVA, female *Jag1*$^{Ndr/Ndr}$ mice vs female controls P=0.0010 and female *Jag1*$^{Ndr/Ndr}$ vs male *Jag1*$^{Ndr/Ndr}$ mice P=0.0286. Male *Jag1*$^{Ndr/Ndr}$ vs controls n.s.). Together, our data demonstrate patterning defects in major arterioles and venules of *Jag1*$^{Ndr/Ndr}$ mice, with sex-specific differences in the numbers of vessels and venous tortuosity.

### *Jag1*$^{Ndr/Ndr}$ *mice display sparse vascular smooth muscle cell coverage of arterioles with large apoptotic gaps in old mice*

Blood vessels are composed of two principal cell types: endothelial cells and mural cells, which include VSMCs and pericytes. The foremost Notch-related vascular disorder CADASIL (caused by mutations in *NOTCH3*) is characterized by poor arterial VSMC coverage and in some cases is associated with neurovascular dementia (*16*). JAG1 also regulates arterial VSMC maturation and maintenance (*13*, *36*) and a ruptured aneurysm in a patient with ALGS suggested VSMC loss

(*37*). We therefore investigated VSMCs and pericytes (a mural cell type required for blood brain/retina barrier integrity (*38*)) in *Jag1*$^{Ndr/Ndr}$ mice and compared these to known CADASIL or *Notch3* mutant phenotypes.

In adult mice, CD13 positive pericytes were not reduced in *Jag1*$^{Ndr/Ndr}$ retinas compared to *Jag1*$^{CTRL}$ retinas (Fig. S4A), comparable to previous reports for *Notch3*$^{-/-}$ mice (*15*). We therefore focused on VSMC development and homeostasis. At P10, α smooth muscle cell actin (αSMA) positive VSMCs covered *Jag1*$^{CTRL}$ arterioles, with VSMCs oriented perpendicular to the blood vessel axis (yellow brackets), while in *Jag1*$^{Ndr/Ndr}$ retinas VSMC were less mature, and some cells exhibited a migratory morphology with their cellular axis parallel to the blood vessel axis (yellow arrows, magnified in inset, Fig. 5A). At P15, αSMA positive VSMCs were fully mature (yellow brackets) in *Jag1*$^{CTRL}$ arterioles, while in *Jag1*$^{Ndr/Ndr}$ retinas VSMC perpendicular coverage was incomplete and parallel-oriented VSMCs were still present (yellow arrows, boxed region, Fig. 5B). Adult *Jag1*$^{Ndr/Ndr}$ mice (at 3 – 6 months) displayed mature but sparse VSMC arteriole coverage (compare broad vs narrow yellow brackets), with clear gaps between VSMCs, and stenoses (green arrowheads, Fig. 5C). Aberrantly oriented VSMCs persist in adult *Jag1*$^{Ndr/Ndr}$ mice (yellow arrow in Fig. 5C). By one year of age, *Jag1*$^{Ndr/Ndr}$ arteriolar VSMCs degenerated, resulting in αSMA-weak (Fig. 5D, blue arrowheads) or negative (Fig. 5D white

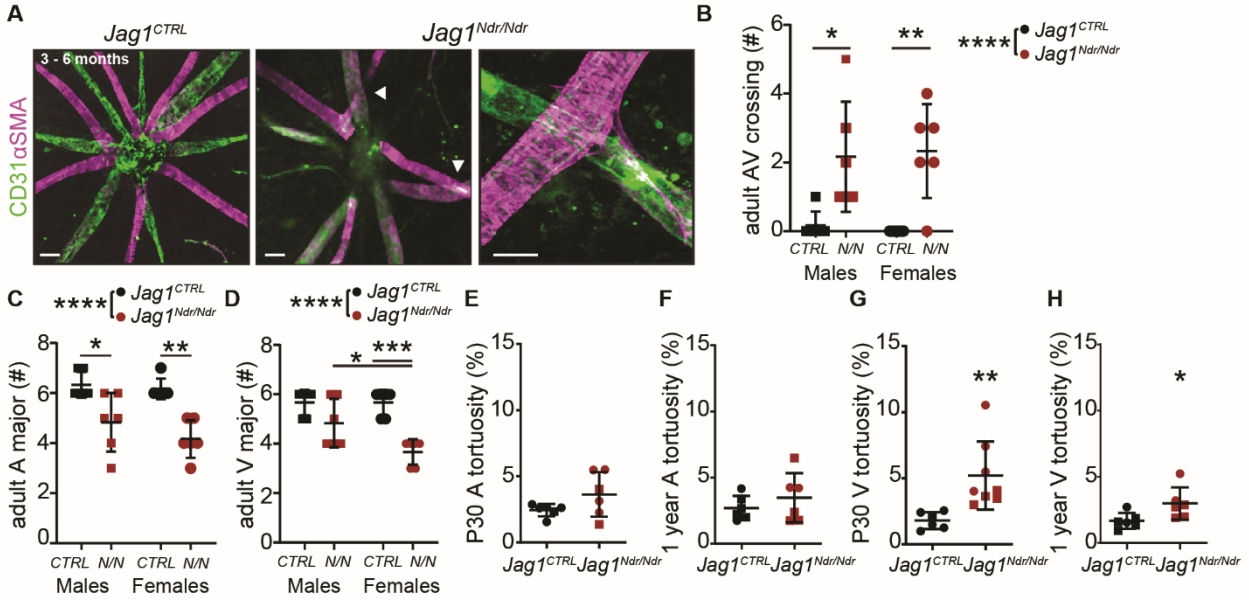


Fig. 4. ***Jag1*$^{Ndr/Ndr}$ mice display vascular guidance defects, with fewer and more tortuous blood vessels. (A)** Radial arrangement of arterioles (magenta) and venules (green) from the optic nerve. White arrowheads label arteriovenous crossings in *Jag1*$^{Ndr/Ndr}$ retina. Scale bar left and middle panel 50 µm, and right panel 20 µm. **(B)** The number of arteriovenous crossings per retina grouped by genotype and sex (n=6 per condition, Two-way ANOVA, genotype ****P<0.0001, followed by Tukey's multiple comparisons test. Male *Jag1*$^{CTRL}$ vs. Male *Jag1*$^{Ndr/Ndr}$ *P=0.0146, Female *Jag1*$^{CTRL}$ vs. Female *Jag1*$^{Ndr/Ndr}$ **P= 0.0061). **(C, D)** Quantification of **(C)** major arterioles (n=6 per condition, Two-way ANOVA genotype ****P<0.0001, followed by Tukey's multiple comparisons test. Male *Jag1*$^{CTRL}$ vs. Male *Jag1*$^{Ndr/Ndr}$ *P=0.0201, Female *Jag1*$^{CTRL}$ vs. Female *Jag1*$^{Ndr/Ndr}$ **P= 0.0011) and **(D)** venules (n=6 per condition, Two-way ANOVA interaction *P=0.0440, sex *P=0.0440, genotype ****P<0.0001, followed by Tukey's multiple comparisons test. Male *Jag1*$^{CTRL}$ vs. Male *Jag1*$^{Ndr/Ndr}$ ns, P= 0.2273, Male *Jag1*$^{Ndr/Ndr}$ vs. Female *Jag1*$^{Ndr/Ndr}$ *P=0.0381, Female *Jag1*$^{CTRL}$ vs. Female *Jag1*$^{Ndr/Ndr}$ ***P=0.0003) originating at the optic nerve head, grouped by genotype and sex. **(E, F)** Arterial tortuosity at **(E)** postnatal day 30 (P30) (n=6 per condition, Unpaired t test, ns, P=0.1276) and at **(F)** 1 year (n=6 per condition, Unpaired t test, ns, P=0.3756). **(G, H)** Measurement of venous tortuosity at **(G)** P30 (*Jag1*$^{CTRL}$ n=6, *Jag1*$^{Ndr/Ndr}$ n=8, Unpaired t test, **P=0.0085, shown in graph, and One-way ANOVA, **P=0.0013, followed by Tukey's multiple comparisons test to test for sex effect, *Jag1*$^{CTRL}$ vs *Jag1*$^{Ndr/Ndr}$ females ***P=0.001, *Jag1*$^{CTRL}$ vs *Jag1*$^{Ndr/Ndr}$ males ns, P=0.2320, *Jag1*$^{Ndr/Ndr}$ females vs *Jag1*$^{Ndr/Ndr}$ males *P=0.0286) and at **(H)** 1 year (n=6 per condition, Unpaired t test, *P=0.0383). Circles represent females, squares represent males. Each dot represents quantifications from one animal; graphs depict mean value ± standard deviation. A, arteriole; AV, arteriovenous; αSMA, alpha smooth muscle actin; F, female; M, male; P(X), postnatal day X; P = , calculated probability; V, venule.

arrowheads) areas. αSMA negative areas were sometimes associated with aneurysms in *Jag1*$^{Ndr/Ndr}$ arterioles (Fig. 5D white arrows, also note the enlarged ECs). To determine whether the sparse VSMC coverage, identified using immunofluorescence, indeed reflected gaps between VSMCs we further analyzed VSMC morphology and arteriolar coverage using transmission electron microscopy of retinal and cardiac blood vessels. Retinal *Jag1*$^{CTRL}$ arteriolar VSMCs were present in a uniform layer surrounding the ECs with wide VSMC-VSMC contacts (Fig. 5E, VSMCs pseudo-colored in magenta and ECs in green, white arrowheads indicate VSMC edges). In contrast, retinal *Jag1*$^{Ndr/Ndr}$ arteriolar VSMCs were

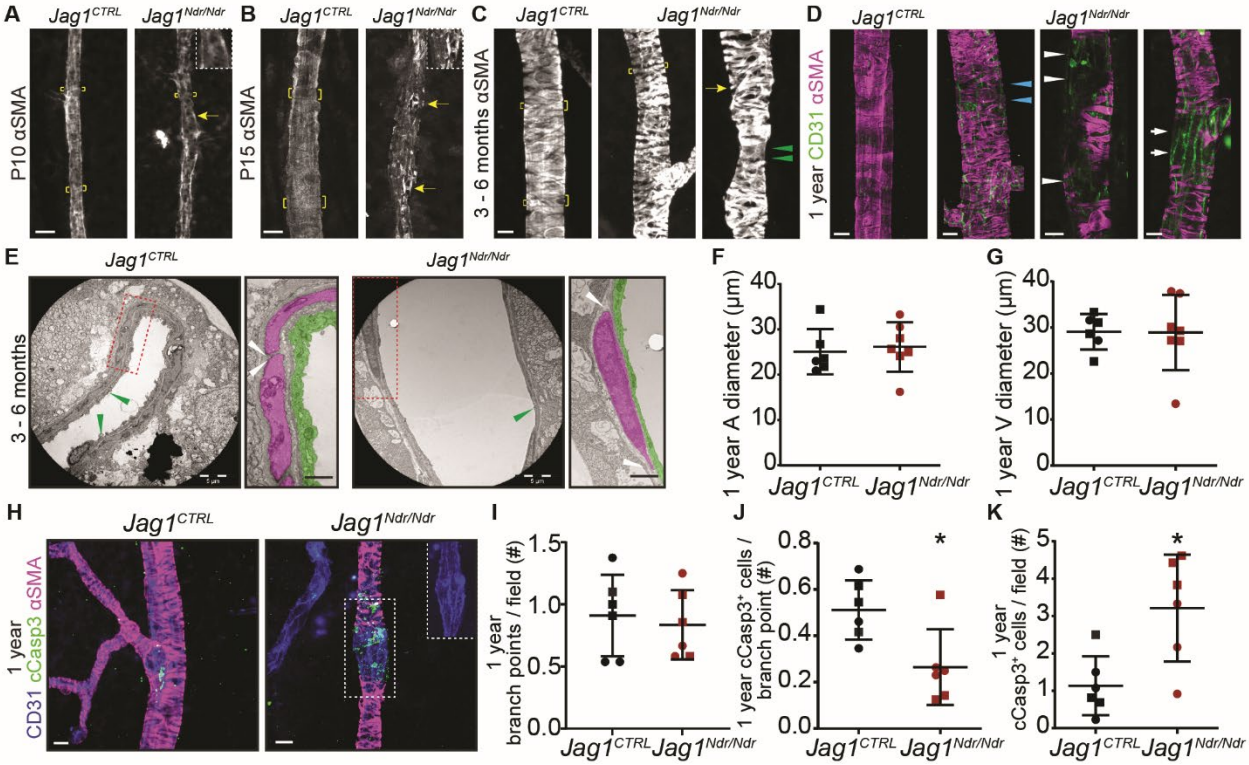


**Fig. 5. *Jag1*$^{Ndr/Ndr}$ mice display sparse vascular smooth muscle cell coverage of arteries with large apoptotic gaps in old mice. (A)** Alpha smooth muscle actin (αSMA) coverage of postnatal day 10 (P10) retinal arterioles (n=6 per condition). Yellow brackets denote horizontal/perpendicular VSMCs, yellow arrow and boxed region highlight vertical/parallel VSMC orientation. In *Jag1*$^{Ndr/Ndr}$ arterioles the VSMCs were oriented parallel to the blood vessel axis, rather than perpendicular and encircling the retinal arteriole. **(B)** αSMA coverage of P15 retinal arterioles (n=6 per condition). Yellow brackets mark horizontal/perpendicular VSMCs, yellow arrows and boxed region highlight a vertical/parallel VSMC. **(C)** Small gaps in αSMA VSMCS coverage of retinal arterioles in 3 – 6 months old mice (n=12 per condition). Green arrowhead denotes focal arterial narrowing/stenosis, yellow arrow highlights a vertical/parallel VSMC. **(D)** αSMA coverage of one-year-old retinal arterioles (n=12 per condition). One-year-old *Jag1*$^{Ndr/Ndr}$ mice arterioles display weaker αSMA coverage (blue arrowheads), αSMA negative gaps (white arrowheads) and an aneurysm (white arrows). Cropped images were placed on a black background for esthetic purposes. Scale bar (A – D) 10 μm. **(E)** Transmission electron microscopy of retinal arterioles. VSMCs color-coded in magenta, endothelial cells (EC) in green. Scale bar 5 μm, boxed region 1 μm. White arrowheads denote the edges of VSMCs and the distance between vascular smooth muscle cells. Green arrowheads denote EC tight junctions. **(F)** Diameter of one-year-old retinal arterioles (n=6 per condition, Unpaired t test, ns, P=0.7276), and **(G)** venules (*Jag1*$^{CTRL}$ n=6 , *Jag1*$^{Ndr/Ndr}$ n=7, Unpaired t test, ns, P=0.9658). **(H)** Cleaved caspase 3 (cCasp3) immunofluorescence staining of apoptotic cells in one-year-old retinal arterioles. Boxed region is a magnification of an aneurysm in a *Jag1*$^{Ndr/Ndr}$ arteriole, note the distended endothelial cells. Scale bar 10 μm. **(I – K)** Quantifications of **(I)** first generation arteriole branching points per field (n=6 per condition, Unpaired t test, ns, P=0.6823) **(J)** number of cCasp3 positive cells associated with a first generation arteriole branching point (n=6 per condition, Unpaired t test, *P=0.0153) and **(K)** number of cCasp3 positive cells per field, excluding those associated with first generation arteriole branching point (n=6 per condition, Unpaired t test, *P=0.0109). Each dot represents one animal; graphs depict mean values ± standard deviation. Circles represent females, squares represent males. A, arteriole; αSMA, alpha smooth muscle actin; cCasp3, cleaved caspase 3; P(X), postnatal day X; P = , calculated probability; V, venule.

sparse, thin, and not in contact with neighboring VSMCs (Fig. 5E, white arrowheads show edges of a VSMC not in contact with another VSMC). These data confirmed that narrow and widely spaced αSMA bands across arterioles (Fig. 5C, 5D) reflected a thinner VSMC layer with fewer contacts. The VSMCs in *Jag1*$^{Ndr/Ndr}$ coronary arteries displayed similar gaps (Fig. S4B, white arrowheads), indicating this VSMC defect is not specific to the nervous system. The tight junctions between ECs were normal in *Jag1*$^{Ndr/Ndr}$ mice (Fig. 5E, Fig. S4B, green arrowheads). Next, we studied arteriolar and venous diameter to determine whether VSMC loss led to changes in vascular tone. No difference in arterial or venous diameter was detected in one-year-old *Jag1*$^{Ndr/Ndr}$ retinas (Figure 5F, 5G).

To investigate whether the VSMC phenotype could be due to altered JAG1 – NOTCH3 levels, we analyzed JAG1 and NOTCH3 protein expression on arterioles (Fig. S4C). JAG1 levels were significantly increased in *Jag1*$^{Ndr/Ndr}$ ECs and VSMCs (Fig. S4C, S4D), in line with our previous report that dysfunctional JAG1$^{NDR}$ accumulates in vivo (*39*). NOTCH3 protein levels were similar in *Jag1*$^{CTRL}$ and *Jag1*$^{Ndr/Ndr}$ arterioles (Fig. S4C, S4E) and *Notch3* mRNA levels were similar in whole retina lysates (Fig. S4F).

To determine whether the changes in VSMC coverage led to reactivity in the parenchyma we evaluated the distribution and morphology of astrocytes. The astrocytes surrounding *Jag1*$^{Ndr/Ndr}$ arterioles were increased in density (Fig. S4G, S4I) and displayed numerous reactive bundles (Fig. S4G, white arrowheads). The astrocytes surrounding venules were similar in distribution in *Jag1*$^{CTRL}$ and *Jag1*$^{Ndr/Ndr}$ retinas (Fig. S4H, S4J).

We next investigated whether the αSMA negative regions in one-year-old mice were due to cells undergoing apoptosis (Fig. 5H. 5K). We quantified the number of cleaved Caspase 3 positive (cCasp3+) cells along the vessels in VSMCs, or associated with a first-generation branching point in ECs, since increased apoptosis was previously shown in VSMCs along the vascular length and in ECs at branch points in *Notch3* mutant mice (*15*). At this stage, the number of first-generation branch points was normal in *Jag1*$^{Ndr/Ndr}$ arterioles (Fig. 5I). Surprisingly, *Jag1*$^{Ndr/Ndr}$ arterioles displayed fewer cCasp3+ ECs at branching points (Fig. 5J) but significantly more cCasp3+ along the arteriole length, often associated with αSMA negative areas (Fig. 5K, note the aneurysm formation in the αSMA negative area, inset in 5H). In sum, *Jag1*$^{Ndr/Ndr}$ arterioles presented with sparse vascular VSMCs that died via apoptosis, sometimes associated with aneurysm formation. Our results thus demonstrate that JAG1 contributed to arteriole VSMC maturation and maintenance.

### *Capillary homeostasis is compromised and retinal ganglion cells break down in Jag1*$^{Ndr/Ndr}$ *retinas*

Blood vessel homeostasis is crucial for the integrity of the blood retina/brain barrier and tissue health, and could be a factor contributing to bleeding in ALGS. A mature vascular plexus is characterized by vessel quiescence (*14*) and by the presence of mural cells, which were abrogated in *Jag1*$^{Ndr/Ndr}$ mice (Fig 5 and Fig. S4). We therefore investigated adult retinal blood vessel homeostasis in *Jag1*$^{Ndr/Ndr}$ mice. We studied all three retinal vascular plexuses in 3 – 6 month old mice, (Fig. 6A), and while the superficial capillary plexus was equally branched in both *Jag1*$^{CTRL}$ and *Jag1*$^{Ndr/Ndr}$ retinas (Fig. 6A, 6B), the *Jag1*$^{Ndr/Ndr}$ intermediate capillary plexus was less vascularized (Fig. 6C) with significantly fewer branching points (Fig. 6D). To understand how age impacted on vasculature in this model, we analyzed all three retinal vascular plexuses in one-year-old mice (Fig. 6E). Both the superficial (Fig. 6F) and the intermediate capillary plexuses were equally branched and vascularized (Fig. 6G, 6H) in *Jag1*$^{CTRL}$ and *Jag1*$^{Ndr/Ndr}$ retinas. The vascularization of the adult (3 – 6 months) *Jag1*$^{Ndr/Ndr}$ retina (Fig. 6B – 6D) was thus similar to the one-year-old *Jag1*$^{CTRL}$ retina (Fig. 6F – 6H) with diminished branching and vascular density in the intermediate capillary plexus.

The vascularization of the intermediate capillary plexus at P15 in *Jag1*$^{Ndr/Ndr}$ retinas was incomplete (Fig. S3B), hence it was not clear

whether the lower vascular length and lower number of branching points in adult *Jag1*$^{Ndr/Ndr}$ retinas reflected a persistence of a developmental defect, or whether capillaries had retracted. When a blood vessel retracts, it leaves behind its basal membrane containing Collagen IV (COLIV) (*13*). In order to determine whether the differences in the

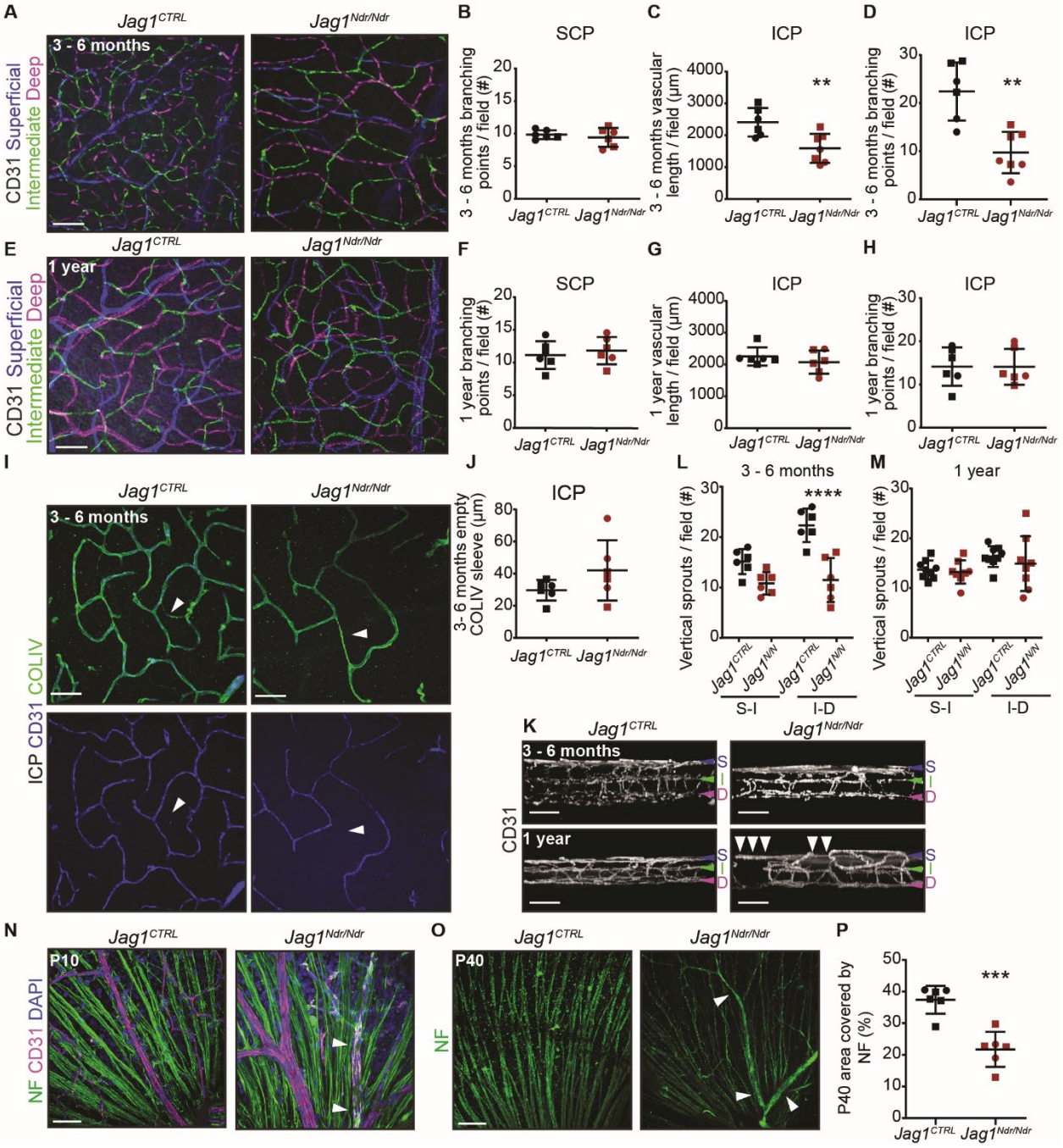


Fig. 6. **Capillary homeostasis is compromised, and retinal ganglion cells break down in *Jag1*$^{Ndr/Ndr}$ retinas. (A)** Pseudocolored classification of the three CD31+ capillary layers in adult retina (3 – 6 months old). Scale bar 50 µm. **(B)** Number of branching points in the superficial capillary plexus (SCP) of adult mice (n=6 per condition, Unpaired t test, ns, P=0.5365). **(C)** Vascular length per field in the intermediate capillary plexus (ICP) in adult mice (n=6 per condition, Unpaired t test, **P=0.0078). **(D)** Number of branching points per field in the ICP in adult mice (n=6 per condition, Unpaired t test, **P=0.001). **(E)** Pseudocolored classification of the three CD31+ capillary layers in one-year-old retina. Scale bar 50 µm. **(F)** Number of branching points per field in SCP in one-year-old mice (n=6 per condition, Unpaired t test, ns, P=0.573). **(G)** Quantification of vascular length per field in ICP in one-year-old mice (n=6 per condition, Unpaired t test, ns, P=0.3686). **(H)** Number of branching points per field in ICP in one-year-old mice (n=6 per condition, Unpaired t test, ns, P=0.9869). (Continued on next page)

intermediate capillary plexus density were a result of capillary regression, we stained for COLIV (Fig. 6I) and measured the lengths of empty COLIV sleeves. Empty COLIV sleeves were increased in the intermediate capillary plexus in two female *Jag1*$^{Ndr/Ndr}$ mice (Fig. 6J), but the overall difference was not statistically significant (P=0.1583). We further quantified the number of vertical sprouts between the superficial and the intermediate (S – I) capillary plexuses and the intermediate and the deep (I – D) capillary plexuses in adult (Fig. 6K, 6L) and one-year-old (Fig. 6K, 6M) mice. The number of I – D vertical sprouts was significantly lower in 3 – 6 month *Jag1*$^{Ndr/Ndr}$ retina compared to the *Jag1*$^{CTRL}$ retina (Fig. 6L). In contrast, the number of vertical sprouts was similar between animals in one-year-old mice (Fig. 6M). Nevertheless, vascular defects were present at both stages as noted by sparse vascular network in 3 – 6 months old *Jag1*$^{Ndr/Ndr}$ retina (Fig. 6K, top panel) and discontinuous intermediate capillary plexus in the one-year-old *Jag1*$^{Ndr/Ndr}$ retina (Fig. 6K, bottom panel, white arrowheads).

The retina is a neural tissue in which retinal ganglion cells (*40*) transmit signals from photoreceptors (rods and cones, the primary light-sensing cells), to the brain via the optic nerve. Approximately 90% of patients with ALGS display optic nerve anomalies such as optic disc drusen, which are hyaline-like calcified nodules (*41*). Retinal ganglion cells, whose cell bodies are located between the superficial and intermediate plexuses, are sensitive to hypoxia and to elevated levels of metabolites in the retina (*42*), suggesting retinal ganglion cells can be affected by the vascular defects identified here. To evaluate if the changes in retinal vasculature had neurological consequences, we investigated retinal ganglion cell axons by staining for neurofilament (NF). The retinal ganglion cells' axons appeared healthy in both *Jag1*$^{CTRL}$ and *Jag1*$^{Ndr/Ndr}$ retinas at P10 (Fig. 6N, white arrowheads label non-specific non-NF immunostaining of blood, due to use of mouse-on-mouse antibody), thus initial development of retinal ganglion cells was not disturbed. However, at P40 the retinal ganglion cells axons in *Jag1*$^{Ndr/Ndr}$ mice were reduced in number (Fig. 6O) and covered 40% less area compared to *Jag1*$^{CTRL}$ mice (Fig. 6P). In conclusion, our results show that the *Jag1*$^{Ndr/Ndr}$ adult vasculature aged prematurely, marked by retracting retinal capillaries resulting in reduced and later discontinued vascular network. The onset of vascular degeneration was associated with retinal ganglion cell degradation in *Jag1*$^{Ndr/Ndr}$ mice.

### *High blood pressure compromises vascular smooth muscle cell homeostasis in Jag1*$^{Ndr/Ndr}$ *mice*

High blood pressure is one of the major risk factors contributing to cardiovascular diseases, subarachnoid hemorrhages and vessel tortuosity (*34*, *43*). Hypertension was reported in several patients with ALGS related to renal artery stenosis (*26*, *44*), or associated with visceral artery aneurysm (*45*), and leads to complications during or after organ transplantation (*46*). *Jag1*$^{Ndr/Ndr}$ mice had significantly lower mean blood pressure (Fig. 7A), ruling out high blood pressure as a cause of abnormal VSMCs and vessel tortuosity. To

Fig. 6. **(Continued) (I)** Immunofluorescence staining of collagen IV (COLIV) and CD31 in ICP identifies regressed COLIV positive/CD31 negative capillaries (arrowheads). Scale bar 50 µm. **(J)** Quantification of empty collagen IV sleeve length per field in ICP (n=6 per condition, Unpaired t test, ns, P=0.1583). **(K)** Side view of all the retinal capillary plexuses in 3 – 6 months old (top panels) and one-year-old mice (bottom panels). The ICP in old *Jag1*$^{Ndr/Ndr}$ mice was discontinuous, labeled by white arrowheads. The SCP is labeled with a blue arrowhead, the ICP with a green arrowhead and the DCP with a magenta arrowhead. **(L, M)** Number of vertical sprouts between SCP (S) and ICP (I) and ICP (I) and DCP (D) in **(L)** adult (n=6 per condition, two-way ANOVA, interaction *P=0.0167, plexus **P=0.0062, genotype ***P=0.0004, followed by Sidak's multiple comparisons test S-I ns, P=0.0592, I-D ****P<0.0001) and **(M)** one-year-old mice (*Jag1*$^{CTRL}$ n=9, *Jag1*$^{Ndr/Ndr}$ n=8, two-way ANOVA, interaction ns, P=0.6334, plexus *P=0.045, genotype ns, P=0.4507, Sidak's multiple comparisons test S-I ns, P=0.9483, I-D ns, P=0.6046). **(N, O)** Retinal ganglion cell axons stained with Neurofilament (NF) at **(N)** postnatal day 10 (P10) and **(O)** P40. Unspecific staining of blood in blood vessels is labelled with white arrowheads. **(P)** Quantification of area covered by NF in P40 mice (n=6 per condition, Unpaired t test, ***P=0.0003). Each dot represents quantifications from one animal; Graphs depict mean values ± standard deviation. Circles represent females, squares represent males. COLIV, collagen IV; D or DCP, deep capillary plexus; I or ICP, intermediate capillary plexus; NF, neurofilament; S or SCP, superficial capillary plexus; P(X), postnatal day X; P = , calculated probability.

investigate whether increased blood pressure impacted on bleeding or vascular health, we treated *Jag1*$^{Ndr/Ndr}$ mice with Angiotensin II (AngII), a VSMC vasoconstrictor, for two weeks (experimental set up Fig. 7B). Hypertension is defined as a systolic blood pressure above 140 mmHg (*47*) (Fig. 7C, dotted line). Responsiveness to AngII was variable, we therefore selected AngII – treated animals with a minimum 20% increase in their mean blood pressure compared to baseline for further study (4 of 9 *Jag1*$^{CTRL}$ mice and 5 of 7 *Jag1*$^{Ndr/Ndr}$ mice, Fig. S5A, S5B, 7C). Of note, *Jag1*$^{CTRL}$ mice tended to lose weight during AngII treatment, while *Jag1*$^{Ndr/Ndr}$ mice increased in weight, resulting in a significant

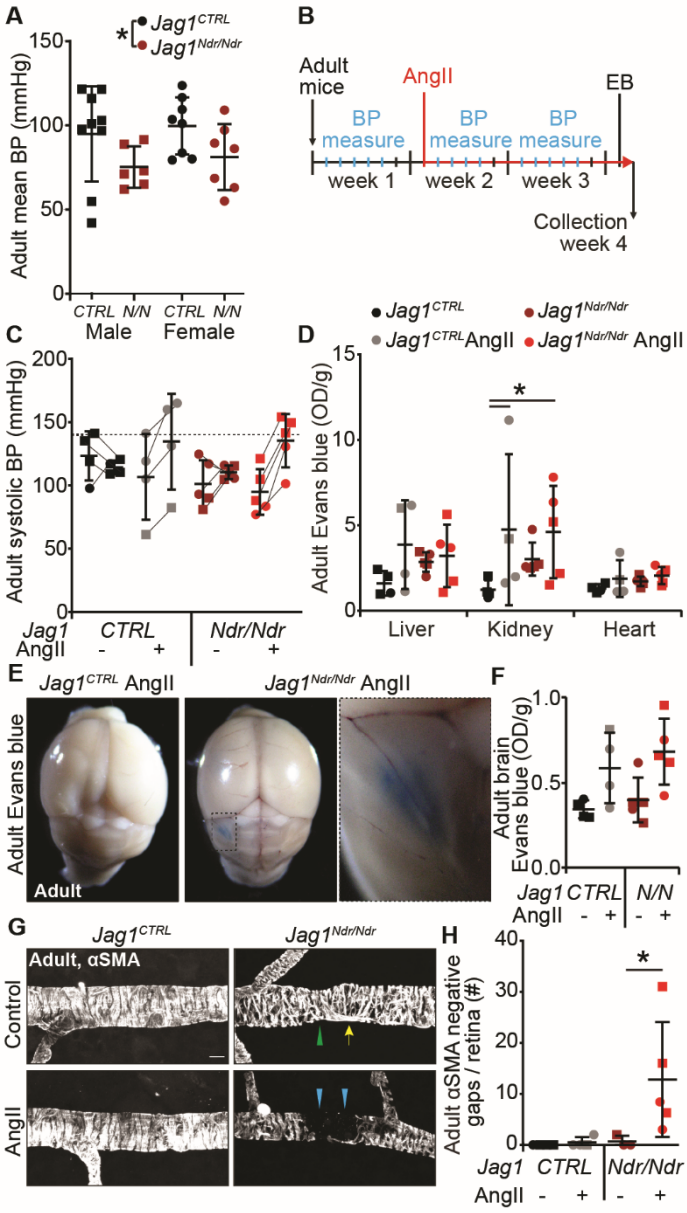


Fig. 7. **High blood pressure compromises vascular smooth muscle cell homeostasis in *Jag1*$^{Ndr/Ndr}$ mice. (A)** Mean blood pressure (BP) measurement in adult mice grouped by genotype and sex (Male *Jag1*$^{CTRL}$ n=9, male *Jag1*$^{Ndr/Ndr}$ n=6, female *Jag1*$^{CTRL}$ n=8, female *Jag1*$^{Ndr/Ndr}$ n=7, Two-way ANOVA, interaction ns, P=0.9407, sex ns, P=0.4957, genotype *P=0.0207, followed by Tukey's multiple comparisons, ns). **(B)** Experimental set up for Angiotensin II treatment. During week one, BP measurements were taken daily (blue tick marks) to establish the baseline levels and habituate the mice to measurements. At the beginning of week two, osmotic pumps with Angiotensin II (+) or PBS control (-) were implanted (red line) and BP was measured daily (blue tick marks). At the beginning of week four, mice were injected with Evans blue (EB) and organs were collected the next day. **(C)** Systolic BP levels before and during Angiotensin II treatment. The thin lines identify the same animal before and during treatment. The dotted line labels the cutoff for hypertension >140 mmHg systolic BP. These data are not tested for significance since animals were explicitly selected for analysis based on their response to Angiotensin, see also Fig. S5. Measurement of Evans blue extracted from liver, kidney and heart (Two-way ANOVA, interaction ns, P=0.2576, organ **P=0.0011, genotype ns; P=0.2086, followed by Tukey's multiple comparisons test with adjusted P-value, all ns except kidney *Jag1*$^{CTRL}$ vs. *Jag1*$^{+/+}$ AngII *P= 0.0383 and *Jag1*$^{CTRL}$ vs. *Jag1*$^{Ndr/Ndr}$ AngII *P=0.0349). **(E)** Qualitative assessment of blood brain barrier permeability with Evans blue after Angiotensin II treatment, in which one *Jag1*$^{Ndr/Ndr}$ mouse (male) of 5 displayed a macroscopically obvious Evans blue leakage. **(F)** Measurement of Evans blue extracted from the brain parenchyma, not including the hemisphere with the major leakage in (E) (Two-way ANOVA, interaction ns, P=0.9687, Treatment/AngII **P=0.007, genotype ns, P=0.5058. Followed by Tukey's multiple comparisons test, all ns. *Jag1*$^{CTRL}$ PBS vs AngII P= 0.0976, *Jag1*$^{Ndr/Ndr}$ PBS vs AngII P= 0.0684). **(G)** Alpha smooth muscle actin (αSMA) coverage of retinal arterioles treated with PBS control or Angiotensin II. The green arrowhead denotes a focal arterial narrowing and the yellow arrow denotes a parallel-oriented VSMC in a *Jag1*$^{Ndr/Ndr}$ mouse. Blue arrowheads label an αSMA negative gap in an Angiotensin II-treated *Jag1*$^{Ndr/Ndr}$ mouse. Scale bar 10 µm. **(H)** Quantification of αSMA negative gaps in arterioles per retina (Two-way ANOVA, genotype, ns, P=0.0747, Sidak's multiple comparison control group ns, P=0.9892, AngII group *P=0.0315). Each dot represents one animal; graphs depict mean values ± standard deviation. Circles represent females, squares represent males. AngII, Angiotensin II; αSMA, alpha smooth muscle actin; BP, blood pressure; EB, Evans blue; OD, optical density.

difference between these two groups (Fig. S5C, S5D).

To evaluate if the increased blood pressure affected blood vessel permeability, we injected the mice with Evans blue. The amount of Evans blue extracted from internal organs was similar in AngII-treated *Jag1*$^{CTRL}$ and *Jag1*$^{Ndr/Ndr}$ mice and was similarly mildly increased compared to the untreated mice (Fig. 7D). Macroscopic evaluation of the brain revealed that one of five AngII-treated *Jag1*$^{Ndr/Ndr}$ mice (a male) displayed Evans blue leakage outside of the intracranial vessels, demonstrating a localized bleed in this animal (Fig. 7E). However, the amount of Evans blue extracted from the brain tissue (excluding the hemisphere with a bleed) was similar in AngII-treated *Jag1*$^{CTRL}$ and *Jag1*$^{Ndr/Ndr}$ mice (Fig. 7F), demonstrating that overall vessel permeability was unaffected.

Finally, we examined whether increased blood pressure affected VSMCs. *Jag1*$^{CTRL}$ VSMCs were not affected by AngII treatment. In contrast, arteriolar αSMA expressing VSMCs in *Jag1*$^{Ndr/Ndr}$ retina were absent in large patches (Fig. 7G, blue arrowheads), resulting in a significant increase in αSMA negative gaps (Fig. 7H), reminiscent of *Notch3*$^{-/-}$ mice at P30 (*15*). In summary, our data show that VSMC homeostasis is compromised in AngII treated *Jag1*$^{Ndr/Ndr}$ mice, leading to gaps in VSMC coverage, and to intracranial vessel leakage in one of five *Jag1*$^{Ndr/Ndr}$ mice.

*Vascular defects identified in Jag1*$^{Ndr/Ndr}$ *mice can be quantified non-invasively in patients with Alagille syndrome using retina fundus photography* Previous reports have shown that patients with ALGS have abnormal retinal vasculature (*48–50*), but the degree of tortuosity and patterning defects have not been quantified, nor compared to animal models, or patients with CADASIL. We first analyzed retinal vasculature in a previously reported cohort of CADASIL patients (*51*, *52*). There were no significant differences in the numbers of arteriovenous crossings (Fig. 8A, 8B), major arterioles or venules (Fig. 8C, 8D) nor in arterial or venous tortuosity (Fig. 8E, 8F) in patients with CADASIL compared to age-matched control patients. Arteriovenous crossings are more common in healthy human retina than in wild type mouse retina (*35*), therefore the observed artery-vein crossings in controls and CADASIL patients were expected. Venous tortuosity was mildly increased in some of the patients with CADASIL, but the degree of tortuosity did not correlate with Fazekas score (a measure of white matter T2 hyperintense lesions used as a proxy for chronic small vessel ischemia, Fig. S6A). While arterial tortuosity does not change with age (Fig. S6B), venous tortuosity appears to correlate with age in healthy humans (Fig. S6C, r = 0.6783, P=0.0077, Fig. S6C), but not in patients with CADASIL (r = 0.1398, P=0.6337).

We analyzed retinal fundus photographs from pediatric patients with ALGS, biliary atresia (BA, as cholestatic controls), and age-matched healthy control patients (previously reported in (*48*, *53*)) (Fig. 8A). Similar to the *Jag1*$^{Ndr/Ndr}$ mice (Fig. 4A, 4B), arteriovenous crossings were significantly increased in patients with ALGS compared to the control group (Fig. 8G). The number of major arterioles and venules were significantly lower in patients with ALGS compared to controls, but similar to patients with BA (Fig. 8H, 8I), indicating that this phenotype (also present in *Jag1*$^{Ndr/Ndr}$ mice in Fig. 4C, 4D) is probably related to cholestasis. Finally, we examined vascular tortuosity, which was consistently increased in *Jag*$^{Ndr/Ndr}$ venules (Fig. 4G, 4H). Arteriole tortuosity was significantly increased in patients with ALGS compared to controls (Fig. 8J), and venule tortuosity was increased in patients with ALGS compared to both patients with BA and healthy controls (Fig. 8K). Interestingly, most patients with ALGS had either very high venous or arterial tortuosity, but rarely both (Fig. S6D). As expected in this small cohort, no patients in this group experienced intracranial bleeds, or bleeding events linked to known vascular abnormalities, and we could therefore not test whether vascular bleeding events correlated with vascular defects. One patient with ALGS had severe bleeding due to coagulopathy (patient f) that was secondary to progressive cholestatic liver disease. Three patients with BA had experienced gastrointestinal bleeding (Table 2). Platelet count (around the time of eye

examination) did not correlate with arteriole or venule tortuosity for patients with ALGS or BA (Fig. S6E, S6F).

Altogether, our data demonstrated that patients with ALGS had vascular abnormalities that could be visualized and quantified non-invasively. Specifically, patients with ALGS

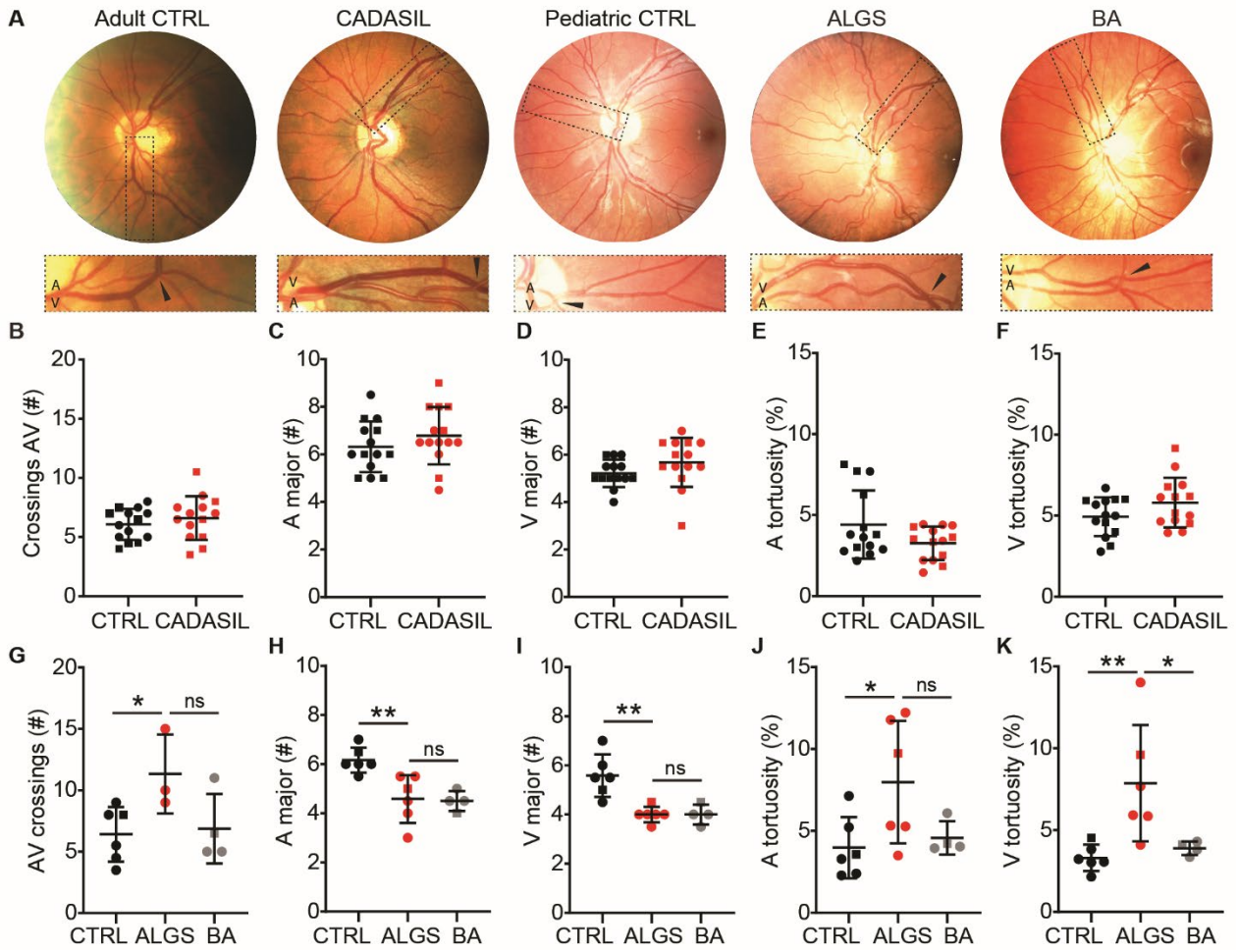


Fig. 8. **Vascular defects identified in *Jag1*$^{Ndr/Ndr}$ mice can be quantified non-invasively in patients with Alagille syndrome using retina fundus photography. (A)** Retinograph examples from a healthy adult individual, a patient with cerebral autosomal dominant arteriopathy with subcortical infarcts and leukoencephalopathy (CADASIL), a healthy pediatric individual, a patient with Alagille syndrome (ALGS) and a patient with biliary atresia (BA, cholestatic control). Boxed regions magnify areas with arteriovenous crossing marked by black arrowheads. **(B)** Number of arteriovenous crossings per retina (n=14 per condition, Unpaired t test, ns, P=0.3854), per person, in Controls and CADASIL patients. **(C, D)** Quantification of **(C)** major arterioles (n=14 per condition, Unpaired t test, ns, P=0.2902) and **(D)** venules (n=14 per condition, Unpaired t test, ns, P=0.1536) at the border of the optic disc per person in Controls and CADASIL patients. **(E, F)** Measurement of **(E)** arterial (n=14 per condition, Unpaired t test, ns, P=0.0759) and **(F)** venous tortuosity (n=14 per condition, Unpaired t test, ns, P=0.1050) in Controls and CADASIL patients. **(G)** Number of arteriovenous crossings per retina in pediatric Controls (n=6), patients with ALGS (n=3), and patients with BA (n=4) (One-way ANOVA, ns, P=0.0608, Sidak's multiple comparisons ALGS vs. CTRL *P=0.0492, ALGS vs. BA ns, P=0.0999). **(H, I)** Quantification of **(H)** major arterioles (One-way ANOVA, **P=0.0026, Sidak's multiple comparisons ALGS vs. CTRL **P=0.0039, ALGS vs. BA ns, P=0.9799) and **(I)** venules (One-way ANOVA, ***P=0.0008, Sidak's multiple comparisons ALGS vs. CTRL *P=0.0011, ALGS vs. BA ns, P>0.9999) at the border of the optic disc in pediatric Controls, patients with ALGS, and patients with BA. **(J, K)** Measurement of **(J)** arterial (One-way ANOVA, *P=0.0486, Sidak's multiple comparisons ALGS vs. CTRL *P=0.0392, ALGS vs. BA ns, P=0.1204) and **(K)** venous tortuosity (One-way ANOVA, **P=0.009, Sidak's multiple comparisons ALGS vs. CTRL **P=0.0076, ALGS vs. BA *P=0.0327) in pediatric Controls, patients with ALGS, and patients with BA. In H-K: CTRLs n= 6, ALGS n= 6, BA n= 4. Each dot represents one individual; graphs depict mean values ± standard deviation. Circles represent females, squares represent males. A, arteriole; ALGS, Alagille syndrome; AV, arteriovenous; BA, biliary atresia; CADASIL, cerebral autosomal dominant arteriopathy with subcortical infarcts and leukoencephalopathy; CTRL, control; V, venule.

have more arteriovenous crossings, fewer major arterioles and venules, and increased vascular tortuosity. Increased venous tortuosity is highly penetrant in patients with ALGS (identified in five of six patients). Importantly, *Jag1*$^{Ndr/Ndr}$ mice predicted these phenotypes with fewer major blood vessels, more arteriovenous crossings, and increased vascular tortuosity.

## Discussion

In this study, we describe multiple roles for *Jag1* in patients and a mouse model for ALGS, in regulating blood vessel growth and homeostasis. We identified risk factors that can lead to bleeds and demonstrated that vascular anomalies can be detected non-invasively in this pediatric population using retinography. We studied vascular anomalies in patients using a systematic literature review and retinography and compared these findings to our investigation of vascular disease and bleeding in the ALGS mouse model. We showed that *Jag1*$^{Ndr/Ndr}$ mice recapitulate spontaneous bleeds, and exhibit arteriovenous crossings, a reduction in blood vessel numbers, and an increase in blood vessel tortuosity, all of which could be confirmed in patient retinographs. Importantly, the systematic review revealed that more female than male patients were reported with idiopathic intracranial bleeding, and female *Jag1*$^{Ndr/Ndr}$ mice displayed more vascular defects than male *Jag1*$^{Ndr/Ndr}$ mice. Although bleeding is sporadic in patients and the mouse model, reduced skull thickness, premature vascular aging, vascular smooth muscle cell degeneration, hypertension, reduced vessel density and increased venous tortuosity indicate multiple risk factors can be present simultaneously in patients. In sum, there are sex-specific differences in *Jag1*-abrogated vasculature, and *Jag1*$^{Ndr/Ndr}$ mice present a faithful model in which to study vascular accidents in ALGS, reproducing phenotypic heterogeneity in de facto bleeds, an absence of coagulopathy, thinning of skull bones, and extensive vascular defects.

Most vascular abnormalities in the systematic review were specific for arteries (Table S1, for example arterial stenoses and aneurysms). Notch signaling is crucial for arterial specification during embryogenesis and arterial smooth muscle cell maintenance throughout life (*15*, *36*). The VSMC paucity and apoptotic VSMCs in the *Jag1*$^{Ndr/Ndr}$ mice is similar to that seen in *Notch3* mutant mice (*15*, *54*), or in the NOTCH3-related disorder CADASIL (*16*). The CADASIL-like VSMC pathology in *Jag1*$^{Ndr/Ndr}$ mice (Fig. 5, 7 and Fig. S4), imply a risk for CADASIL-like vascular dementia in patients with ALGS. CADASIL is typically thought of as an arteriopathy affecting the brain but vascular defects in CADASIL are systemic, and present in both arteries and veins (*55*, *56*), prompting the suggestion that this should be thought of as a vasculopathy or angiopathy instead (*56*). Although *Jag1* is thought of as being expressed in arterial ECs, *Jag1* is in fact expressed in both arterial and venous VSMCs at high levels, and in both venous and arterial ECs (*57*). In *Jag1*$^{Ndr/Ndr}$ mice, VSMC paucity was present in cardiac and neural arterioles (Fig. 5E and Fig S4B), and both arterioles and venules were tortuous in patients with ALGS (Fig. 8J, 8K). We have also previously shown that the intrahepatic portal venous system is tortuous (*20*). Our data thus demonstrate that ALGS and *Jag1*$^{Ndr/Ndr}$ vascular defects are systemic and present in both arteries and veins. Surprisingly, the retinal vascular abnormalities found in patients with ALGS were not detected in retinographs from patients with CADASIL, although some individuals with CADASIL displayed elevated venous tortuosity compared to the control group. Venous tortuosity increased with age in control patients (Fig. S6C) therefore vessel tortuosity is likely most informative in younger patient groups. Vascular changes in CADASIL patients, including arterial and venous dilation and reduced vessel density, have been identified using optical coherence tomography angiography (OCTA) (*51*, *52*), and future studies of patients with ALGS using OCTA would be useful to further investigate pathologies non-invasively. It is thus likely that abrogation of Notch signaling by defective *JAG1* in ALGS, or defective *NOTCH3* in CADASIL, leads to systemic defects in veins and arteries, that have the biggest functional impact on arteries that are subjected to the greatest strain, resulting in aneurysm rupture or

stroke. Whether venous or arterial tortuosity can be used as correlates for general vascular health in patients thus warrants further investigation in larger patient cohorts. Weak VSMC coverage in a ruptured intracranial aneurysm in patient with ALGS (*37*), further corroborates that VSMC pathology is of concern in ALGS. VSMC health can be compromised by hypertension, indicating that patients' blood pressure should be monitored carefully. Hypertension can lead to severe cardiovascular health complications including stroke, heart attack or intracranial hemorrhage (*43*). Hypertension was reported in several patients with ALGS often related to renal artery stenosis (*26*, *44*, *58*) and associated with visceral artery aneurysm (*45*). Two weeks of hypertension in *Jag1*$^{Ndr/Ndr}$ mice caused rapid degeneration of VSMCs, forming αSMA-negative gaps in the VSMC layer, while the wild type VSMCs were unaffected. Hypertension could thus be a major risk factor for patients with ALGS. Future studies should therefore aim to systematically determine whether VSMC compromise in patients with ALGS interacts with elevated blood pressure (as our results in mice show), and how this is similar or dissimilar to CADASIL.

Retinal vascular changes are correlated with cerebral small vessel disease (*59*). Furthermore, vessel tortuosity is a general indicator of vessel wall dysfunction (*60*) and is associated with ischemic stroke (*61*), while arteriovenous nicking is associated with hemorrhagic stroke (*62*). Retinal vessel tortuosity is also associated with hypertension, diabetes, genetic disorders, hypoxia-related retinopathies, and ischemic heart disease (*63–65*). Tortuosity of vessels can arise due to vessel wall weakening, leading to dilation and elongation of blood vessels (usually weakening of the tunica intima/ECs, but sometimes also tunica media/VSMCs). Abnormal retinal vessels are correlated with other abnormal vessels in the body (*50*), and non-invasive retinal vascular imaging could thus serve as a screening method to investigate vascular compromise in patients with ALGS. Retinal tortuosity in patients with ALGS (Fig. 8) should therefore be further investigated as a correlate for neurovascular dolichoectasia in patients with ALGS (*9*) or with tortuous vessels in lung (Dieulafoy lesions) which are linked to pulmonary hemorrhage in patients with ALGS (Fig 1B, Table S1).

Aging is a major risk factor contributing to the development of cardiovascular disease and is partly attributed to vessel wall changes leading to EC dysfunction (*66*) and loss of contractile VSMCs (*67*). Retinal vascular health was severely affected in adult (3 – 6 months old) *Jag1*$^{Ndr/Ndr}$ mice as shown by decreased vascular density and sparse VSMC coverage. Specifically, the number of branching points in the intermediate capillary plexus and the number of vertical sprouts in the adult *Jag1*$^{Ndr/Ndr}$ mice were similar to one-year-old wild type mice, indicating a premature aging-like phenotype. Reduced retinal vessel branching is also present in patients with ALGS (*49*) and was apparent in the retina fundus photographs from patients with ALGS (Fig. 8), with fewer major arterioles and venules at the optic disc border. In the general population, ruptured intracranial aneurysms occur between 56 – 58 years of age (*30*), whereas the age range for intracranial hemorrhage in patients with ALGS was 2 months to 30 years old (Table 1). Premature vascular aging in patients with ALGS could also explain early-onset vascular bleeding.

Our systematic review identified ten females and one male with ALGS and idiopathic intracranial bleeds (Table 1, Fig 1B). The majority of these were subarachnoid hemorrhages (SAH), which is more common in men than women between age 25-45, but is more common in women than men between age 55-85 (*25*). The greater risk of SAH in women over 55 has been speculated to relate to hormonal differences after menopause, but hormone replacement therapy has yielded mixed results (*68*, *69*). Patients with ALGS may also present with hormonal differences, which are as yet poorly characterized: delayed puberty in seen in some patients with ALGS, as well as non-reponsiveness to growth hormone (*70*, *71*). The patients summarized in the systematic review, with SAH, were older (the male was 13 years old, the females were 9-30 years old), while the younger patients with brain bleeds could generally be explained by coagulopathy

or minor trauma. Whether hormones interact with the risk of SAH in this pediatric population is thus worth further investigation.

Patients with ALGS exhibit several ocular abnormalities, of which the most common optic disc anomaly is optic disc drusen (*41*), which compresses adjacent ganglion cell axons and promotes retrograde axonal degeneration (*72*). Our data suggest that vascular pathology in the JAG1-mutant retina leads to local tissue hypoxia, negatively influencing the surrounding neurons, especially the retinal ganglion cells, which could explain the high incidence of optic disc drusen in ALGS patients. Fortunately, even though ALGS patients display many ocular abnormalities, complete vision loss is very rare (*73*). However, monitoring retinal vasculature and the development of optic disc drusen could also be investigated as a prognostic marker for systemic vascular anomalies.

Our data demonstrate that multiple risk factors likely interact to contribute to bleeding in patients with ALGS, and that these pathologies are possible to study in the *Jag1*$^{Ndr/Ndr}$ mouse model (impact of sex, skull thinning and both EC and VSMC defects). Our data indicate that efforts should be made to identify and monitor patients that are at a greater risk of vascular disease (e.g. females with ALGS, aged 15 – 30 years old, who appear to have higher risk of idiopathic intracranial bleeding, or hypertensive patients with ALGS) and highlight the need for screening patients with ALGS for vascular and neurovascular changes. Future studies should aim to identify the patients with ALGS at greatest risk of vascular disease, and devise treatments for vascular defects in this disease. *Jag1*$^{Ndr/Ndr}$ mice present a suitable tool for pre-clinical trials of vascular intervention therapies, which could draw inspiration from the field of CADASIL, also aiming at treating VSMC compromise.

## Materials and Methods

### Experimental design

The objective of this study was to identify risk factors and sex differences underlying vascular abnormalities in patients with ALGS and whether they can be modeled in *Jag1*$^{Ndr/Ndr}$ mice. We performed a systematic review to map which vascular abnormalities were most common in patients with ALGS and whether there were any sex differences. We used whole mount immunohistochemistry, confocal microscopy, and transmission electron microscopy to study vascular cellular changes during development, homeostasis and aging in *Jag1*$^{Ndr/Ndr}$ mice. We assessed coagulation status with functional assays in P10 mice, and we measured cranial thickness using microCT. Finally, we analyzed retinal fundus photographs from patients with ALGS, BA or CADASIL as well as age-matched controls to determine whether vascular defects identified in *Jag1*$^{Ndr/Ndr}$ mice could be identified non-invasively in patients with ALGS.

### Systematic review search strategy

The Medline (Ovid), Embase and Web of Science Core Collection database were used for publication search. After the initial search, automated deduplication was performed by the Karolinska Institutet library. The databases were searched on three occasions up to June 14$^{th}$, 2021. Two reviewers screened, reviewed and collected each record independently. The systematic review followed the Prisma 2000 guidelines (*27*).

Records that had no abstract available in English and publications that were not accessible were excluded. Publications that were included in the systematic review contained information about the ALGS diagnosis, patient sex and vascular events except for pulmonary artery stenosis, which is a hallmark of ALGS. Patients that explicitly did not meet the criteria for diagnosis (genetically confirmed, or presenting three of five diagnostic features, or relatives of confirmed cases with at least two hallmarks) were excluded. Additional reasons for exclusion were bleeding as a consequence of hepatocellular carcinoma, displaced blood vessels secondary to other primary defects, splenic hamartoma (benign splenic mass, not thought of as a vascular lesion), or aortic stenosis stated to be a consequence of a bicuspid valve. Non-peer reviewed abstracts from conferences were included. Structural abnormalities and vascular events were

tabulated for all reports. Structural abnormalities quantified included stenosis, collateral vessel or occlusion, aneurysm, Moyamoya, vessel agenesis or hypoplasia, vessel wall abnormality, skin vessel abnormality, vascular bruits and persistent falcine sinus. Vascular events included ischemic or hemorrhagic events or post-surgical vascular complications. The findings of the studies were tabulated and compared for males and females. If a study contained a vascular abnormality that was not part of any group of the synthesis, the patient's information was included only in the patient overview table (Table S1). After the full screen by two reviewers, the two independent lists were compared and discussed to identify any mismatches and determine final inclusion/exclusion.

Articles with relevant vascular information but lacking sex data were pursued by contacting study authors for more information. None of the study authors were able to provide sex data where this was missing from the original publication.

Data are presented as summary of reported events in males and females and the difference between males and females was tested using two-tailed binominal exact test. For observed vs expected outcomes, a 1:1 distribution of cases between males and females was assumed to be expected.

Search strategy for Medline:

Field labels: exp/ = exploded MeSH term; / = non exploded MeSH term; .ti,ab,kf. = title, abstract and author keywords; adjx = within x words, regardless of order; * = truncation of word for alternate endings

1. Alagille Syndrome/
2. (alagill* adj3 (syndrome* or watson or disease)).ti,ab,kf.
3. (watson miller or arteriohepatic dysplasia or cardiovertebral syndrome or hepatic ductular hypoplasia or hepatofacioneurocardiovertebral or cholestasis with peripheral pulmonary stenosis or paucity of interlobular bile ducts or hepatic ductular hypoplasia).ti,ab,kf.
4. or/1-3
5. exp Cardiovascular System/ab, pa [Abnormalities, Pathology]
6. exp Vascular Diseases/
7. exp Hemorrhage/
8. exp Vascular Malformations/
9. (vascula* or cerebrovasc* or stroke* or aneurysm* or blood vessel* or artery or arteries or vein* or venous or moyamoya or moya moya or bleed* or hemorrhag*).ti,ab,kf.
10. or/5-9
11. 4 and 10
12. remove duplicates from 11

Search strategy for Embase:

Field labels: /exp = exploded Emtree term; /de = non exploded Emtree term; ti,ab = title and abstract; NEAR/x = within x words, regardless of order; * = truncation of word for alternate endings

(('alagille syndrome'/de) OR ((alagill* NEAR/3 (syndrome* OR watson OR disease)):ti,ab,kw) OR ('watson miller':ti,ab,kw OR 'arteriohepatic dysplasia':ti,ab,kw OR 'cardiovertebral syndrome':ti,ab,kw OR hepatofacioneurocardiovertebral:ti,ab,kw OR 'cholestasis with peripheral pulmonary stenosis':ti,ab,kw OR 'paucity of interlobular bile ducts':ti,ab,kw OR 'hepatic ductular hypoplasia':ti,ab,kw))

AND

(('cardiovascular system'/exp AND (abnormal* OR patholog*)) OR ('vascular disease'/exp) OR ('bleeding'/exp) OR (vascula*:ti,ab,kw OR cerebrovasc*:ti,ab,kw OR stroke*:ti,ab,kw OR aneurysm*:ti,ab,kw OR 'blood vessel*':ti,ab,kw OR artery:ti,ab,kw OR arteries:ti,ab,kw OR vein*:ti,ab,kw OR venous:ti,ab,kw OR moyamoya:ti,ab,kw OR 'moya moya':ti,ab,kw OR bleed*:ti,ab,kw OR hemorrhag*:ti,ab,kw))

Search strategy for Web of Science Core Collection:

Field labels: TS/Topic = title, abstract, author keywords and Keywords Plus; NEAR/x = within x words, regardless of order; * = truncation of word for alternate endings

TS=(alagill* NEAR/3 (syndrome* OR watson OR disease)) OR TS=("watson miller" OR "arteriohepatic dysplasia" OR "cardiovertebral syndrome" OR hepatofacioneurocardiovertebral OR "cholestasis with peripheral pulmonary stenosis" OR "paucity of interlobular bile ducts" OR "hepatic ductular hypoplasia")

AND

TS=(vascula* OR cerebrovasc* OR stroke* OR aneurysm* OR "blood vessel*" OR artery OR arteries OR vein* OR venous OR moyamoya OR "moya moya" OR bleed* OR hemorrhag*)

## Mouse maintenance and breeding

Animal experiments were performed in accordance with local rules and regulations and were approved by Stockholms Norra Djurförsöksetiska nämnd (Stockholm animal research ethics board, ethics approval numbers: N50/14, N61/16, N5253/19, N2987/20, N14960/2020). The Nodder (*Jag1*$^{+/Ndr}$ colony) mice were maintained in a mixed C3H/C57bl6 genetic background as reported previously (*19*). In brief, *Jag1*$^{+/Ndr}$ mice are maintained in a C3H background (EMMA C3HeB/FeJ-Jag1$^{Ndr}$/Ieg, EM: 13207) and outbred to C57bl6 for experiments. *Jag1*$^{Ndr/Ndr}$ mice are obtained from heterozygous crossings, and where possible littermates are used as controls. Nodder mice were genotyped for the *Ndr* allele and sex by Transnetyx® (USA). Mice were housed in cages with enrichment and maintained on a standard day-night (12 hour) cycle, with ad libitum access to food (standard chow SDS RM3 or SDS CRM, Special Diet Services) and water. Experiments generally include mice of both male and female sex. Experiments in which the results suggested sex differences were expanded with additional mice of each sex to determine whether sex differences were present. *Jag1*$^{+/+}$ and *Jag1*$^{Ndr/+}$ mice display wild type vasculature, and *Jag1*$^{Ndr/+}$ mice have not displayed spontaneous bleeds, and are thus both used as controls (*Jag1*$^{CTRL}$). The use of each genotype is specified in each section below.

## Patient samples

Color photographs of the ocular fundii of patients with ALGS, BA and their age-matched controls were obtained after pupil dilatation using fundus cameras Canon EOS-1 Kodak Professional DCS 520C (Canon, Rochester, New York, USA) or Canon CRDG non-mydriatic retinal camera (Canon, Tokyo, Japan). Only correctly focused photographs either from eyes with both the macula and the optic disc visible, or from eyes with the optic disc in the center, were used for the analysis. Data collection and analysis was performed under the 335/00, and 2019-00202 ethical permits approved by Regional ethics review board in Stockholm. Seven healthy pediatric control patients (median age 8 years, range 7 – 8 years; 1 male, 6 females), six patients with ALGS (median age 7.5 years, range 2 – 11 years; 1 male, 5 females), four patients with BA (median age 10.5 years, range 8 – 16 years; 1 male, 3 females) were included. The patients included in this study and/or their guardians gave written informed consent, and were previously reported in part (*48*, *53*).

Color fundus photography of patients with CADASIL and their aged-matched controls was performed using Visucam (Carl Zeiss Meditech, Germany). The data collection and analysis were approved by the IRB of the Ärztekammer Westfalen-Lippe and University of Münster (2015-402-f-S). All subjects gave written informed consent. Data from these patients have been published in part in previous studies (*51*, *52*). Fourteen healthy adult control patients (median age 48 year, range 23 – 61 years; 5 males, 9 females) and 14 patients with CADASIL (median age 51 year, 6 males, 8 females) were included.

The medical history from patients with ALGS or BA, whose retina fundus photographs were analyzed here, follows the decision 2017/1394-31 by the Regional ethics review board in Stockholm. Permission was given to retrospectively collect data from charts of patients with chronic cholestatic disease without additional consent from patients.

## Immunofluorescence staining of retina

Eyes were fixed with 3.8% Formaldehyde solution (Sigma-Aldrich, cat. #F1635) overnight and whole retinas were dissected out, blocked and permeabilized in phosphate buffered saline (PBS) containing 1% Bovine serum albumin (Sigma-Aldrich, cat. # A2153) with 0.3% TritonX-100 (Sigma-Aldrich, cat. #T8787). Primary and secondary antibodies were diluted in blocking solution. PBS : blocking solution (1:1) was used as a washing buffer. Each step was performed at 4°C, overnight. Retinas were flat-mounted in Vectashield (cat. no. H-1000, Vector Laboratories). Primary antibodies used: rat anti-mouse CD31 (cat. #553370, BD Biosciences, 1:100), rabbit anti-ERG (cat. #ab92513, Abcam, 1:200), goat-anti DLL4 (cat. #AF1389, RnD systems, dilution 1:200), goat anti-CD13 (cat. #AF2335, RnD Systems), goat anti-Jagged1 (cat. #J4127, Sigma-Aldrich, 1:500), mouse anti-human α-smooth muscle actin (Cy3 conjugated, cat. #C6198, Sigma Aldrich, 1:500; FITC conjugated, cat. #F3777, Sigma Aldrich, 1:500), rabbit anti-HISTONE H3 (phospho S10) (cat. #ab5176, Abcam, 1:500), rabbit anti-NOTCH3 (cat. #Ab23426, Abcam, 1:500), mouse anti-GFAP (Cy3 conjugated, cat. # MAB3402C3, Sigma-Aldrich, 1:500), rabbit anti-Cleaved CASPASE3 (cat. #9661 (D175), Cell Signaling, 1:700), rabbit anti-COLLAGEN type IV (cat. # AB756P, Merck Millipore, 1:500), mouse anti-Neurofilament (cat. #RT97, DSHB, 1:200) nuclei were labeled with DAPI (cat. #D9542, Sigma Aldrich, 1:1000). Images were captured using LSM 510 META, LSM 880, LSM980 (Carl Zeiss AG) microscopes and processed in Image J (NIH), and/or Adobe image suite software (Adobe Inc). Any image modifications were applied identically to images being compared.

## Quantitative analysis of the retinal vasculature

### Vascular outgrowth analysis

The distance from the optic nerve to the periphery of a retina was measured in ImageJ (NIH) using the straight line tool. Distance was measured on tile-scanned images (10x or 20x objective) of whole retina starting from the optic nerve. 6 measurements, regularly radially spaced at approximately 60 degree intervals, were performed per retina from 6 $Jag1^{+/+}$ and 6 $Jag1^{Ndr/Ndr}$ animals at P5 and 7 $Jag1^{+/+}$ and 7 $Jag1^{Ndr/Ndr}$ at P4 (for DLL4 neutralizing antibody experiments).

### Tip cells and filopodia analysis

Tip cells were defined as $CD31^{+}Erg^{+}$ cells with extended filopodia at the vascular front. The number of tips per tip cell was quantified as the number of tips with filopodia bundles (single membrane protrusions coming out of a tip cell) extending in a single direction, divided by the number of tip cells. Filopodia was defined as single hair-like membrane protrusions extending from a tip cell. The number of filopodia was then divided either by the number of tip cells or by the number of tips. All quantifications were counted manually in Image J, in 40x images, 4 images per animal, in 6 $Jag1^{+/+}$ and 6 $Jag1^{Ndr/Ndr}$ mice at P5.

### Quantification of vascular density, branching point and number of ERG+ endothelial cells

The number of branching points per field (40x objective) was manually quantified in the middle of the outgrowing vascular plexus (at P4, P5, P10, P15, adult and 1 year halfway between an arteriole and venule). The quantification of branching points was performed in 3 - 6 images per animal, in 7 $Jag1^{+/+}$ and 7 $Jag1^{Ndr/Ndr}$ mice at P4, 6 $Jag1^{+/+}$ and 6 $Jag1^{Ndr/Ndr}$ mice at P5 and P15, 4 $Jag1^{+/+}$, 2 $Jag1^{Ndr/+}$ and 6 $Jag1^{Ndr/Ndr}$ mice at P10 and 5 $Jag1^{+/+}$, 1 $Jag1^{Ndr/+}$ and 6 $Jag1^{Ndr/Ndr}$ mice adult mice (3 – 6 months) and aged animals (1 year). In each 40x field the number of $ERG^{+}$ nuclei were manually quantified in 3 – 5 images per animal, in 6 $Jag1^{+/+}$ and 6 $Jag1^{Ndr/Ndr}$ mice at P5 and P15, 4 $Jag1^{+/+}$, 2 $Jag1^{Ndr/+}$ and 6 $Jag1^{Ndr/Ndr}$ mice at P10. In the same field, the CD31+ vascular length was manually measured using the free hand or segmented line tool in ImageJ. The number of ERG+ endothelial cells was divided by vascular length.

### Phosphorylated Histone3 proliferation analysis

Whole retina tile-scans (objective 10x) were taken from 4 *Jag1*$^{+/+}$ and 4 *Jag1*$^{Ndr/Ndr}$ mice at P5, and 3 *Jag1*$^{+/+}$ and 3 *Jag1*$^{Ndr/Ndr}$ mice at P10 and P15. Phospho-Histone H3+ (PH3+) CD31+ cells were manually counted in a field within a 45° wedge originating at the optic nerve, in zones of radius 200 µm, in 12 zones altogether (Supp Figure 1D). The average number of PH3+CD31+ per zone was normalized to the zone area (µm$^2$) and multiplied by 100 (per 100 µm$^2$ area).

**Vessel diameter analysis**

Vessel diameter was measured at 220 µm and 440 µm from the optic nerve in ImageJ, and averaged, for all major arterioles and venules in 4 *Jag1*$^{+/+}$, 2 *Jag1*$^{Ndr/+}$ and 6 *Jag1*$^{Ndr/Ndr}$ mice at 1 year.

**Cleaved Caspase 3**

The number of cleaved caspase3 (Cl. CASP3) positive cells was quantified manually along arterioles in aged mice (>1 year old) in 7 – 13 stacks per mouse, in 5 *Jag1*$^{+/+}$, 1 *Jag1*$^{Ndr/+}$ and 6 *Jag1*$^{Ndr/Ndr}$ mice. The arterioles were imaged in confocal z-stacks and inspected for cl. CASP3+ cells throughout the stacks. The number of first generation arteriole branching points per image (field), the number of cl. CASP3+ cells at a branching point and the number of cl. CASP3+ outside of a branching point were manually quantified.

**Arterial and venous segregation**

In murine retinas, the number of major arterioles and venules originating at the optic nerve, and the number of arteriovenous crossings, were quantified in whole mount retinas stained for CD31 and αSMA. 6 male and 6 female *Jag1*$^{+/+}$ and 6 male and 6 female *Jag1*$^{Ndr/Ndr}$ adults were included for quantification of arterioles and venules. Arteriole/arteriole and arteriole/venule crossings were counted and grouped together. No venule/venule crossings were observed. Altogether 6 male and 6 female *Jag1*$^{+/+}$ mice and 6 male and 6 female *Jag1*$^{Ndr/Ndr}$ mice were included for quantification of aberrant crossings in adult mice (3 – 6 months).

In human retinas, the number of major arterioles and venules were quantified at the border of the optic nerve head from fundus photographs in which the optic nerve head was the center of the image. The venules were recognized by their darker color. The number of arteriovenous crossings was counted. No distinction was made between arteriovenous crossing and nicking. Patients with ALGS – 3, BA – 4, pediatric control – 6, CADASIL – 14, adult control – 14.

**Vessel tortuosity**

Blood vessel tortuosity was quantified by manually tracing the curved length of major arterioles and venules from the optic nerve towards the periphery in murine whole retina (20x objective) or human retina fundus photographs, in Adobe Illustrator or ImageJ. In murine retinas, only the main branches were traced for analysis. In human retinas, only branches that extended to the periphery (edge of the image) were included for analysis. The chord length was measured as a straight line connecting the start point to the end point of a vessel. Tortuosity was calculated by dividing the curved length by the chord length, and expressed as a percentage increase over 100% (100% = straight). The analysis was performed on whole retinas from one eye from 6 *Jag1*$^{+/+}$ and 8 (6 for arterioles) *Jag1*$^{Ndr/Ndr}$ P30 mice, 6 *Jag1*$^{+/+}$ and 6 *Jag1*$^{Ndr/Ndr}$ one-year-old mice and all the patients included in the study (both eyes).

**Vertical sprouting analysis**

To address the overall number of sprouts connecting SCP to ICP, and DCP to ICP, a single image from a z-stack halfway between SCP to ICP and DCP to ICP was analyzed. A sprout in this image appears as a single dot. One to three Z-stack images (40x objective) taken in the middle of a retina between arteriole and venule was analyzed per animal. 6 *Jag1*$^{+/+}$ and 6 *Jag1*$^{Ndr/Ndr}$ adult mice (3 – 6 months) and 9 *Jag1*$^{+/+}$ and 8 *Jag1*$^{Ndr/Ndr}$ aged animals (one year) were included.

**Superficial and intermediate capillary plexus integrity**

The number of SCP and ICP branching points was quantified in z-projected images (ImageJ) of the SCP or ICP (40x objective) taken in the middle of the retina between an arteriole and a venule. Four images from 6 *Jag1*$^{+/+}$ and 7 *Jag1*$^{Ndr/Ndr}$ adult animals, and 2 - 5 images from 6 *Jag1*$^{+/+}$ 6 *Jag1*$^{Ndr/Ndr}$ one-year-old animals were analyzed. In the same field, the CD31+ vascular length was measured by free hand tool in ImageJ. In the intermediate capillary plexus in 6 *Jag1*$^{+/+}$ and 6 *Jag1*$^{Ndr/Ndr}$ adult animals (3 – 6 months), the length of empty CollagenIV sleeves was measured using the free hand or segmented line tool in ImageJ.

### Neurofilament quantification

Neurofilament coverage was quantified in ImageJ and calculated as % of area covered by neurofilaments of the total area (100%). Neurofilament area was measured using the following script in ImageJ:

```
run("Measure");
run("8-bit");
run("Median...", "radius=2");
setAutoThreshold("Mean dark");
//run("Threshold...");
//setThreshold(6, 255);
setOption("BlackBackground", false);
run("Convert to Mask");
run("Watershed");
run("Analyze Particles...");
```

Total area was measured with “Measure”.

The measurement was performed on 2-4 images from 6 *Jag1*$^{+/+}$ and 6 *Jag1*$^{Ndr/Ndr}$ P40 animals.

### Fluorescence intensity

The blood vessel of interest was outlined using the lasso tool. The intensity was assessed by the histogram function for individual channels in Adobe Photoshop.

GFAP intensity was quantified in adults from 3 images from 4 *Jag1*$^{+/+}$ and 4 *Jag1*$^{Ndr/Ndr}$ mice.

JAG1 intensity was quantified in adults from 4 images from 4 *Jag1*$^{+/+}$ and 4 *Jag1*$^{Ndr/Ndr}$ mice.

NOTCH3 intensity was quantified in adults from 4 images from 4 *Jag1*$^{+/+}$ and 4 *Jag1*$^{Ndr/Ndr}$ mice.

### ASMA gaps

The number of gaps in αSMA coverage was quantified manually. An αSMA gap was considered a gap between two vascular smooth muscle cells that is greater than one cell width (~ >10 µm). The total number of gaps per retina was counted. The number of gaps was quantified in 4 *Jag1*$^{+/+}$, 3 *Jag1*$^{Ndr/Ndr}$, 4 *Jag1*$^{+/+}$ treated with Angiotensin II and 5 *Jag1*$^{Ndr/Ndr}$ treated with Angiotensin II.

### Whole organ hemorrhage analysis and imaging

Freshly dissected lungs, brains retinas were inspected for the presence of hemorrhages under a stereomicroscope Stemi 305 (Carl Zeiss Microscopy). Whole organs or tissue images were taken with a stereomicroscope Stemi 305 (Carl Zeiss Microscopy) combined with Canon camera (Cannon, PowerShot S3 IS or Iphone6). The background around the tissue (brain, retina) was covered by a solid black color in Adobe Photoshop for esthetic purposes.

### Image processing

Capillary plexus visualization was accomplished by splitting z-stack images into 3 equally sized z-stacks per animal, color coding each plexus and merging the 3 images. Due to different sizes of *Jag1*$^{+/+}$ and *Jag1*$^{Ndr/Ndr}$ retinas, stack sizes were different among animals. Some images (Fig. 3N, 4A, 6E, Fig. S3A) were further processed in ImageJ by median filter (radius = 1).

Retina whole vasculature side images were further processed in Volocity in which high opacity and noise reduction filters were included.

### Liver resin casting

Adult liver portal vein vasculature was injected with synthetic resin MICROFIL® and scanned

with micro computed tomography as previously described (*22*).

### Micro CT analysis of ruptures

Following the micro-CT measurements, the reconstructed data was imported in VG Studio MAX software (Volume Graphics GmbH, https://www.volumegraphics.com). The Microfil-filled structures were separated from the background by global thresholding creating a main region of interest (ROI), then the areas of Microfil leaked from ruptured vessels were manually selected into separate ROIs. The volume of each ROI of leaked Microfil was calculated by the software. The analysis was performed in 4 $Jag1^{+/+}$, 2 $Jag1^{+/Ndr}$ and 6 $Jag1^{Ndr/Ndr}$ samples (analyses of portal vein and biliary architecture, but not vascular leakage data, for 3 $Jag1^{+/+}$ and 3 $Jag1^{Ndr/Ndr}$ samples of these casts were previously published in (*22*)).

### Skull micro computed tomography

Micro-computed tomography (microCT) was performed on 7- and 8-month-old skulls, 6 $Jag1^{+/+}$ and 6 $Jag1^{Ndr/Ndr}$ mice using a MicroCT50 (Scanco Medical), 55kVp, 109µA, 6W at 20µm voxel size, with a 500 ms integration time and a 20.5 mm field of view.

### Skull thickness and volume analysis

The skull thickness and volume analyses were conducted in VG Studio MAX 3.4 (Volume Graphics GmbH, Germany). A sample was registered within the coordinate system, and the skull surface was determined, including the jaws. The volume was calculated by multiplying the number of voxels of a given surface by the volume of one voxel. The skull thickness was measured by utilizing a ray, searching for the opposite surface for each point on the skull surface. The resulting thickness map depicts the shortest distances between the inner and outer surface. The thickness and volume of the skulls were measured in two different ways, one of the whole skull thickness and one taking into account the trabeculation of the spongy bone. The spongy bone segmentation was conducted using the VGEasyPore module. The analysis was performed in 6 $Jag1^{+/+}$, 6 $Jag1^{Ndr/Ndr}$ adult samples (all males).

### Skull length

The skull length was measured in Image J using the straight line tool. The length was measured from the occipital bone to the nasal bone from a dorsal view. The measurement was performed for 6 $Jag1^{+/+}$, and 6 $Jag1^{Ndr/Ndr}$ skulls.

### Vessel permeability assay

Mice were injected with 200 µl 0.5% Evans blue (cat. #E2153, Sigma-Aldrich) via the tail vein. The dye was allowed to circulate for 17 hours. Mice were anesthetized by CO2 inhalation. Mice were either transcardially perfused with Hanks buffered salt solution (HBSS), at a perfusion rate of 5 ml/min for 3 min, or organs were immediately collected. Internal organs were dissected out, weighed, and placed in matched volumes of Formamide solution (cat. # 15515-026, Invitrogen) for 17 hours at 56°C. Formamide solution containing Evans blue thus extracted from the organs was measured for absorbance at 610 nm in a VersaMax™ microplate reader (Molecular Devices Versa Max microplate reader). The amount of Evans blue measured was divided by the organ weight, and data were normalized to control conditions for either perfused or unperfused conditions, as appropriate. Brain vasculature was inspected under the stereomicroscope Stemi 305 (Carl Zeiss Microscopy) and photographed with a camera (Cannon, PowerShot S3 IS). The analysis is based on 5 $Jag1^{+/+}$, 2 $Jag1^{+/Ndr}$ and 8 $Jag1^{Ndr/Ndr}$ mice.

### Blood pressure measurements

Blood pressure was measured using the CODA® High Throughput (Kent Scientific) tail cuff system. The animals were awake, on a heating pad, and in a restraining device, during the experiment. The animals were accustomed to the tail cuff for 5 min before data recording. Tail blood pressure was assessed between 32 – 34°C. The systolic, diastolic and mean blood pressure were recorded. The mean baseline blood pressure was calculated as an average

from 5 recordings on 5 days. In the Angiotensin II experiment, the mean blood pressure is the average of nine recordings. The increase in blood pressure was calculated by comparing the average mean blood pressure before Angiotensin II treatment (100%) and during two weeks of Angiotensin II treatment.

## Angiotensin II treatment

Adult mice (3-7.5 months) were treated with Angiotensin II (cat. #A6402, Sigma-Aldrich) for two weeks. Angiotensin II was delivered via osmotic mini pumps (Alzet®, 2002 model) with an infusion rate of 0.025 µg/g/h. The animals were anesthetized by Isoflurane inhalation (~2%) and IP injected with 200 µl Rimadyl (0.5 mg/ml) prior to the surgery to relieve pain. The osmotic mini pumps were implanted subcutaneously and the incision was sealed with surgical glue. Animals in the experiment were weighed daily and the blood pressure was measured to verify the effect of Angiotensin II treatment. 2 of 11 *Jag1*$^{+/+}$ mice, and 1 of 8 *Jag1*$^{Ndr/Ndr}$ mice demonstrated a strong reaction to Angiotensin II treatment (weight loss > 20% and piloerection) and had to be sacrificed. 5 *Jag1*$^{+/+}$ and 2 *Jag1*$^{Ndr/Ndr}$ mice had weak or no response to Angiotensin II (no blood pressure increase) and were therefore excluded from the analysis. Animals were given extra "porridge" during the treatment to avoid dehydration. Control animals were implanted with mini-pumps loaded with Dulbecco´s phosphate buffer saline (DPBS), in total 4 *Jag1*$^{+/+}$ and 5 *Jag1*$^{Ndr/Ndr}$ mice.

## Body weight

*Jag1*$^{+/+}$ and *Jag1*$^{Ndr/Ndr}$ body weight was recorded from the first day of blood pressure measurement and throughout the Angiotensin II treatment. In the body weight graph, day 0 is body weight before the Angiotensin II treatment and day 1 is body weight from the first day of Angiotensin II treatment. Body weight change is calculated by comparing the body weight from the last day of Angiotensin II treatment to the body weight from the first day of AngII treatment (100%).

## Plasma and serum collection

Blood from P10 mice was collected from the trunk after decapitation. To obtain blood plasma the blood was mixed with 10 µl of Heparin (LEO Pharma) and kept cold throughout handling. To obtain serum the blood was collected in a tube and allowed to coagulate at room temperature. Afterwards, the blood-Heparin mix was centrifuged at 3000 g for 15 min at 4°C (plasma) or blood was centrifuged at 3000 g for 15 min at room temperature (serum). Plasma or serum was carefully removed from the top layer, placed in a new tube, and frozen (-20°C short term (max 2 weeks), -80°C long term storage). Blood plasma was collected from 6 *Jag1*$^{+/+}$ and 6 *Jag1*$^{Ndr/Ndr}$ mice and serum were collected from 6 *Jag1*$^{+/+}$ and 6 *Jag1*$^{Ndr/Ndr}$ mice.

## Coagulation assays

Thrombin-Antithrombin (TAT) complexes were measured in blood plasma by ELISA using a commercial kit (cat. #ab137994, Abcam). The assay was performed according to manufacturer's instructions. The chromogen substrate was incubated for 20 min and the absorbance was read at 450 nm using VersaMax™ microplate reader. The TAT ELISA was performed on P10 plasma (6 *Jag1*$^{+/+}$ and 6 *Jag1*$^{Ndr/Ndr}$ mice).

Fibrinogen was measured in P10 serum (6 *Jag1*$^{+/+}$ and 6 *Jag1*$^{Ndr/Ndr}$ mice) using a commercial kit (cat. #ab213478, Abcam), according to manufacturer's instructions. The chromogen substrate was incubated for 15 min and the absorbance was read at 450 nm using VersaMax™ microplate reader.

INR was measured in a drop of fresh whole blood (6 *Jag1*$^{+/+}$ and 6 *Jag1*$^{Ndr/Ndr}$ mice at P10) with a commercially available point of care coagumeter (CoaguChek® XS, Roche).

Tail bleeding time was assessed in 6 *Jag1*$^{+/+}$ and 6 *Jag1*$^{Ndr/Ndr}$ mice at P10 in anesthetized (Isoflurane inhalation) pups by severing the tip of the tail (2mm from the tip) and gently wiping the tail on a tissue paper without squeezing the tail. The time was recorded from the moment the tail was cut. The tail was wiped every 20 s to observe the bleeding. The bleeding was

considered stopped when no bleeding reappeared after 1 min.

### Liver enzyme analysis

Liver enzymes (including total bilirubin) were analyzed from blood plasma of 6 *Jag1*$^{+/+}$ and 6 *Jag1*$^{Ndr/Ndr}$ mice P10 mice diluted sixfold with DPBS, using mammalian liver profile (Abaxis, PN 500-1040) and VetScan2 system (Abaxis Inc).

### Survival analysis

Newborn pups were observed and live/deceased mice were counted daily during the first 10 days after birth. The pups were biopsied, tattooed and genotyped. 23 *Jag1*$^{+/+}$ and 16 *Jag1*$^{Ndr/Ndr}$ were included in the analysis, 6 *Jag1*$^{Ndr/Ndr}$ pups died during the first 10 days.

### Electron microscopy

Animals were anesthetized and transcardially perfused with HBSS and electron microscopy fixative (2% formaldehyde, 2.5% glutaraldehyde and 0.02% sodium azide in 0.05 M sodium cacodylate buffer, pH 7.2) as previously described (*15*). For retina and heart analysis 6 *Jag1*$^{+/+}$ and 6 *Jag1*$^{Ndr/Ndr}$ mice were used. Images were further processed in Adobe Photoshop to pseudocolor cell types.

### Quantitative real time qPCR

RNA was isolated from 6 *Jag1*$^{+/+}$ and 6 *Jag1*$^{Ndr/Ndr}$ P5 pups and 3 *Jag1*$^{+/+}$ and 3 *Jag1*$^{Ndr/Ndr}$ adult mice. mRNA was extracted using the RNeasy Mini Kit (QIAGEN, cat. #74104), including on-column DNase I digestion (QIAGEN, cat. #79254). Complementary DNA was synthesized from 1 µg total RNA using the Thermo Scientific™ Maxima™ First Strand cDNA Synthesis Kit for RT-qPCR (Thermo Scientific, cat. #K1641) according to the manufacturer instructions. Quantitative real-time PCR (qPCR) was performed as described (*74*). Primers used for qPCR are listed below. mRNA levels are normalized to the average housekeeping RNA levels of 18S and β-actin.

| Gene | Forward primer | Reverse primer | Product length (bp) |
|---|---|---|---|
| 18S | gtggagcgatttgtctggtt | cgctgagccagtcagtgtag | 200 |
| β-actin | gacaggatgcagaaggagat | ttgctgatccacatctgctg | 146 |
| Dll4 | tttgcccagactccatcctcacag | ttccccccatctcccttattgg | 356 |
| Notch3 | tgagtgtccagctggctatg | cacaggtgccattgtgtagg | 224 |

### DLL4 neutralizing antibody treatment

Newborn pups were injected at P2 via the temporal vein with 0.0025mg/g of DLL4-neutralizing (blocking antibody (YW152F, Genentech (*31*)) or IgG from human serum (cat #I4506, Sigma Aldrich). The pups were sacrificed 48 h after injection at P4. 4 *Jag1*$^{+/+}$ and 4 *Jag1*$^{Ndr/Ndr}$ mice were injected with IgG and 3 *Jag1*$^{+/+}$ and 3 *Jag1*$^{Ndr/Ndr}$ mice were injected with DLL4-blocking antibody.

### Statistical analysis

Statistical analyses of differences between *Jag1*$^{CTRL}$ and *Jag1*$^{Ndr/Ndr}$ animals was evaluated using two-sided unequal variance *t*-test or Mann-Whitney test. When more than 2 conditions were compared, a one-way ANOVA was used, and when two grouping variables were being analyzed (eg genotype and another variable), a two-way ANOVA combined with Sidak's multiple comparisons test was used, as appropriate and as described in figure legends. Pearson correlation was used for correlation analysis. For analysis of the systematic review, two-sided binominal exact test was used to test whether the observed proportions of male and female patients, reported with given vascular or bleeding events, was significantly different

from the expected proportions (1:1). *P* value was considered statistically significant if $p<0.05$ ($p<0.05$ = *, $p<0.01$ = **, $p<0.0001$ = ***. Specific P-values listed in figure legends).

## References


1. D. Alagille, M. Odièvre, M. Gautier, J. P. Dommergues, Hepatic ductular hypoplasia associated with characteristic facies, vertebral malformations, retarded physical, mental, and sexual development, and cardiac murmur. *J. Pediatr.* **86**, 63–71 (1975).
2. K. M. Emerick, E. B. Rand, E. Goldmuntz, I. D. Krantz, N. B. Spinner, D. A. Piccoli, Features of Alagille syndrome in 92 patients: frequency and relation to prognosis. *Hepatology*. **29**, 822–829 (1999).
3. B. M. Kamath, N. B. Spinner, K. M. Emerick, A. E. Chudley, C. Booth, D. A. Piccoli, I. D. Krantz, Vascular Anomalies in Alagille Syndrome: A Significant Cause of Morbidity and Mortality. *Circulation*. **109**, 1354–1358 (2004).
4. R. E. Quiros-Tejeira, M. E. Ament, M. B. Heyman, M. G. Martin, P. Rosenthal, T. R. Hall, S. V McDiarmid, J. H. Vargas, Variable morbidity in alagille syndrome: a review of 43 cases. *J. Pediatr. Gastroenterol. Nutr.* **29**, 431–437 (1999).
5. P. Lykavieris, C. Crosnier, C. Trichet, M. Meunier-Rotival, M. Hadchouel, Bleeding tendency in children with Alagille syndrome. *Pediatrics*. **111**, 167–170 (2003).
6. E. J. Hoffenberg, M. R. Narkewicz, J. M. Sondheimer, D. J. Smith, A. Silverman, R. J. Sokol, Outcome of syndromic paucity of interlobular bile ducts (Alagille syndrome) with onset of cholestasis in infancy. *J. Pediatr.* **127**, 220–4 (1995).
7. R. Kazi, J. Fakhoury, R. Beck, A Case of Recurrent Intracranial Bleeds in the Setting of Alagille Syndrome. *Pediatrics*. **142** (2018), doi:10.1542/peds.142.1_MeetingAbstract.52.
8. A. Petaros, D. Miletic, S. Stifter, M. Slaus, V. Stemberga, Alagille syndrome case report: implications for forensic pathology and anthropology. *Int. J. Legal Med.* **129**, 543–549 (2015).
9. C. D. Carpenter, L. L. Linscott, J. L. Leach, S. Vadivelu, T. Abruzzo, Spectrum of cerebral arterial and venous abnormalities in Alagille syndrome. *Pediatr. Radiol.* **48**, 602–608 (2018).
10. L. Li, I. D. Krantz, Y. Deng, A. Genin, A. B. Banta, C. C. Collins, M. Qi, B. J. Trask, W. L. Kuo, J. Cochran, T. Costa, M. E. M. Pierpont, E. B. Rand, D. A. Piccoli, L. Hood, N. B. Spinner, Alagille syndrome is caused by mutations in human Jagged1, which encodes a ligand for Notch1. *Nat Genet*. **16**, 243–51. (1997).
11. T. Oda, A. G. Elkahloun, B. L. Pike, K. Okajima, I. D. Krantz, A. Genin, D. A. Piccoli, P. S. Meltzer, N. B. Spinner, F. S. Collins, S. C. Chandrasekharappa, Mutations in the human Jagged1 gene are responsible for Alagille syndrome. *Nat. Genet.* **16**, 235–242 (1997).
12. R. McDaniell, D. M. Warthen, P. A. Sanchez-Lara, A. Pai, I. D. Krantz, D. A. Piccoli, N. B. Spinner, NOTCH2 mutations cause Alagille syndrome, a heterogeneous disorder of the notch signaling pathway. *Am. J. Hum. Genet.* **79**, 169–73 (2006).
13. R. Benedito, C. Roca, I. Sörensen, S. Adams, A. Gossler, M. Fruttiger, R. H. Adams, The notch ligands Dll4 and Jagged1 have opposing effects on angiogenesis. *Cell*. **137**, 1124–35 (2009).
14. L. K. Phng, H. Gerhardt, Angiogenesis: A Team Effort Coordinated by Notch. *Dev. Cell*. **16**, 196–208 (2009).
15. T. L. Henshall, A. Keller, L. He, B. R. Johansson, E. Wallgard, E. Raschperger, M. Andaloussi Mae, S. Jin, C. Betsholtz, U. Lendahl, Notch3 is necessary for blood vessel integrity in the central nervous system. *Arterioscler. Thromb. Vasc. Biol.* **35**, 409–420 (2015).
16. A. Joutel, C. Corpechot, A. Ducros, K. Vahedi, H. Chabriat, P. Mouton, S. Alamowitch, V. Domenga, M. Cécillion, E. Marechal, J. Maciazek, C. Vayssiere, C. Cruaud, E. A. Cabanis, M. M. Ruchoux, J. Weissenbach, J. F. Bach, M. G. Bousser, E. Tournier-Lasserve, Notch3 mutations in CADASIL, a hereditary adult-onset condition causing stroke and dementia. *Nature*. **383**, 707–710 (1996).
17. J. Mašek, E. R. Andersson, The developmental biology of genetic Notch disorders. *Development*. **144**, 1743–1763 (2017).
18. C. Crosnier, T. Attié-Bitach, F. Encha-Razavi, S. Audollent, F. Soudy, M. Hadchouel, M. Meunier-Rotival, M. Vekemans, JAGGED1 gene expression during human embryogenesis elucidates the wide phenotypic spectrum of Alagille syndrome. *Hepatology*. **32**, 574–81 (2000).
19. E. R. Andersson, I. V Chivukula, S. Hankeova, M. Sjöqvist, Y. L. Tsoi, D. Ramsköld, J. Masek, A. Elmansuri, A. Hoogendoorn, E. Vazquez, H. Storvall, J. Netušilová, M. Huch, B. Fischler, E. Ellis, A. Contreras, A. Nemeth, K. C. Chien, H. Clevers, R. Sandberg, V. Bryja, U. Lendahl, Mouse Model of Alagille Syndrome and Mechanisms of Jagged1 Missense Mutations. *Gastroenterology*. **154**, 1080–1095 (2018).
20. S. Hankeova, J. Salplachta, T. Zikmund, M. Kavkova, V. Hul, A. Brinek, V. Smekalova, J. Laznovsky, U. Lendahl, E. Ellis, A. Nemeth, DUCT reveals architectural mechanisms contributing to bile duct recovery in a mouse model for Alagille syndrome. *Elife*. **10**, 1–29 (2021).
21. C. S. Teng, H.-Y. Yen, L. Barske, B. Smith, J. Llamas, N. Segil, J. Go, P. A. Sanchez-Lara, R. E. Maxson, J. G. Crump, Requirement for Jagged1-Notch2 signaling in patterning the bones of the mouse and human middle ear. *Sci. Rep.* **7**, 2497 (2017).
22. P. S. Kawada, A. Bruce, P. Massicotte, M. Bauman, J. Yap, Coagulopathy in Children with Liver Disease. *J. Pediatr. Gastroenterol. Nutr.* **65**, 603–607 (2017).
23. J. W. Haukeland, M. C. Småstuen, P. P. Pålsdatter, M. Ismail, Z. Konopski, K. K. Jørgensen, H. Lannerstedt, H. Midgard, Effect of gender on mortality and causes of death in cirrhotic patients with gastroesophageal varices. A retrospective study in Norway. *PLoS One*. **15** (2020), doi:10.1371/JOURNAL.PONE.0230263.
24. P. Appelros, B. Stegmayr, A. Terent, Sex differences in stroke epidemiology: A systematic review. *Stroke*. **40**, 1082–1090 (2009).
25. N. K. de Rooij, F. H. H. Linn, J. A. van der Plas, A. Algra, G. J. E. Rinkel, Incidence of subarachnoid haemorrhage: a systematic review with emphasis on region, age, gender and time trends. *J. Neurol. Neurosurg. Psychiatry*. **78**, 1365–1372 (2007).
26. K. M. Emerick, I. D. Krantz, B. M. Kamath, C. Darling, D. M. Burrowes, N. B. Spinner, P. F. Whitington, D. A. Piccoli, Intracranial vascular abnormalities in patients with Alagille syndrome. *J. Pediatr. Gastroenterol. Nutr.* **41**, 99–107 (2005).
27. M. J. Page, J. E. McKenzie, P. M. Bossuyt, I. Boutron, T. C. Hoffmann, C. D. Mulrow, L. Shamseer, J. M. Tetzlaff, E. A. Akl, S. E. Brennan, R. Chou, J. Glanville, J. M.

Grimshaw, A. Hróbjartsson, M. M. Lalu, T. Li, E. W. Loder, E. Mayo-Wilson, S. McDonald, L. A. McGuinness, L. A. Stewart, J. Thomas, A. C. Tricco, V. A. Welch, P. Whiting, D. Moher, The PRISMA 2020 statement: an updated guideline for reporting systematic reviews. *Syst. Rev. 2021 101*. **10**, 1–11 (2021).

28. S. Yilmaz, T. Turhan, S. Mutluer, S. Aydogdu, The Association of Alagille Syndrome and Craniosynostosis. *Pediatr. Neurol.* **48**, 146–148 (2013).
29. A. Stahl, K. M. Connor, P. Sapieha, J. Chen, R. J. Dennison, N. M. Krah, M. R. Seaward, K. L. Willett, C. M. Aderman, K. I. Guerin, J. Hua, C. Löfqvist, A. Hellström, L. E. H. Smith, The mouse retina as an angiogenesis model. *Investig. Ophthalmol. Vis. Sci.* **51**, 2813–2826 (2010).
30. G.-X. Wang, D. Zhang, Z.-P. Wang, L.-Q. Yang, H. Yang, W. Li, Risk factors for ruptured intracranial aneurysms. *Indian J. Med. Res.* **147**, 51–57 (2018).
31. J. Ridgway, G. Zhang, Y. Wu, S. Stawicki, W.-C. Liang, Y. Chanthery, J. Kowalski, R. J. Watts, C. Callahan, I. Kasman, M. Singh, M. Chien, C. Tan, J.-A. S. Hongo, F. de Sauvage, G. Plowman, M. Yan, Inhibition of Dll4 signalling inhibits tumour growth by deregulating angiogenesis. *Nature*. **444**, 1083–1087 (2006).
32. C. Z. Qiao, G. T. Richter, W. J. Pan, Y. B. Jin, X. X. Lin, Extracranial arteriovenous malformations: from bedside to bench. *Mutagenesis*. **34**, 299–306 (2019).
33. T. W. Secomb, Hemodynamics. *Compr. Physiol.* **6**, 975–1003 (2016).
34. H. C. Han, Twisted blood vessels: Symptoms, etiology and biomechanical mechanisms. *J. Vasc. Res.* **49**, 185–197 (2012).
35. G. Martin, K. L. Wefelmeyer, F. Bucher, G. Schlunck, H. T. Agostini, Arteriovenous crossing in retinal vessels of mice, rats, and pigs. *Mol. Vis.* **26**, 731–741 (2020).
36. F. A. High, M. M. Lu, W. S. Pear, K. M. Loomes, K. H. Kaestner, J. A. Epstein, Endothelial expression of the Notch ligand Jagged1 is required for vascular smooth muscle development. *Proc. Natl. Acad. Sci. U. S. A.* **105**, 1955–9 (2008).
37. E. Doberentz, K. Kuchelmeister, B. Madea, Subarachnoid hemorrhage due to aneurysm rupture in a young woman with Alagille syndrome - A rare cause of sudden death. *Leg. Med. (Tokyo).* **17**, 309–312 (2015).
38. A. Armulik, G. Genove, M. Mäe, M. H. Nisancioglu, E. Wallgard, C. Niaudet, L. He, J. Norlin, P. Lindblom, K. Strittmatter, B. R. Johansson, C. Betsholtz, Pericytes regulate the blood–brain barrier. *Nat. Lett.* **468**, 557–561 (2010).
39. E. M. Hansson, F. Lanner, D. Das, A. Mutvei, U. Marklund, J. Ericson, F. Farnebo, G. Stumm, H. Stenmark, E. R. Andersson, U. Lendahl, Control of Notch-ligand endocytosis by ligand-receptor interaction. *J. Cell Sci.* **123**, 2931–42 (2010).
40. J. R. Sanes, R. H. Masland, The Types of Retinal Ganglion Cells: Current Status and Implications for Neuronal Classification. *Annu. Rev. Neurosci.* **38**, 221–246 (2015).
41. N. M. El-Koofy, R. El-Mahdy, M. E. Fahmy, A. El-Hennawy, M. Y. Farag, H. M. El-Karaksy, Alagille syndrome: clinical and ocular pathognomonic features. *Eur. J. Ophthalmol.* **21**, 199–206 (2011).
42. H. Kergoat, M.-E. Herard, M. Lemay, RGC Sensitivity to Mild Systemic Hypoxia. *Investig. Ophthalmol. Vis. Sci.* **47**, 5423–5427 (2006).
43. M. J. O'Donnell, D. Xavier, L. Liu, H. Zhang, S. L. Chin, P. Rao-Melacini, S. Rangarajan, S. Islam, P. Pais, M. J. McQueen, C. Mondo, A. Damasceno, P. Lopez-Jaramillo, G. J. Hankey, A. L. Dans, K. Yusoff, T. Truelsen, H.-C. Diener, R. L. Sacco, D. Ryglewicz, A. Czlonkowska, C. Weimar, X. Wang, S. Yusuf, Risk factors for ischaemic and intracerebral haemorrhagic stroke in 22 countries (the INTERSTROKE study): a case-control study. *Lancet*. **376**, 112–123 (2010).
44. E. Berard, J. Sarles, V. Triolo, M. F. Gagnadoux, F. Wernert, M. Hadchouel, P. Niaudet, Renovascular hypertension and vascular anomalies in Alagille syndrome. *Pediatr Nephrol.* **12**, 121–124 (1998).
45. Y. Sanada, I. Naya, T. Katano, Y. Hirata, N. Yamada, N. Okada, Y. Ihara, Y. Onishi, K. Mizuta, Visceral artery anomalies in patients with Alagille syndrome. *Pediatr. Transplant.* **23**, e13352.
46. B. M. Kamath, N. B. Spinner, N. D. Rosenblum, Renal involvement and the role of Notch signalling in Alagille syndrome. *Nat. Rev. Nephrol.* **9**, 409–18 (2013).
47. C. Johns, I. Gavras, D. E. Handy, S. Abrahao, G. Haralambos, Models of Experimental Hypertension in Mice. *Hypertension*. **28**, 1064–1069 (1996).
48. K. T. Fahnehjelm, B. Fischler, L. Martin, A. Nemeth, Occurrence and pattern of ocular disease in children with cholestatic disorders. *Acta Ophthalmol.* **89**, 143–150 (2011).
49. M. Hingorani, K. K. Nischal, A. Davies, C. Bentley, A. Vivian, A. J. Baker, G. Mieli-Vergani, A. C. Bird, W. A. Aclimandos, Ocular Abnormalities in Alagille Syndrome. *Ophthalmology*. **106**, 330–337 (1999).
50. B. J. Kim, A. B. Fulton, The genetics and ocular findings of Alagille syndrome. *Semin. Ophthalmol.* **22**, 205–10 (2007).
51. F. Alten, J. Motte, C. Ewering, N. Osada, C. R. Clemens, E. M. Kadas, N. Eter, F. Paul, M. Marziniak, Multimodal retinal vessel analysis in CADASIL patients. *PLoS One*. **9**, 1–10 (2014).
52. P. Nelis, I. Kleffner, M. C. Burg, C. R. Clemens, M. Alnawaiseh, J. Motte, M. Marziniak, N. Eter, F. Alten, OCT-Angiography reveals reduced vessel density in the deep retinal plexus of CADASIL patients. *Sci. Rep.* **8**, 1–7 (2018).
53. K. T. Fahnehjelm, K. Wide, J. Ygge, A. Hellström, T. Tomson, B. Winbladh, K. Strömland, Visual and ocular outcome in children after prenatal exposure to antiepileptic drugs. *Acta Ophthalmol. Scand.* **77**, 530–535 (1999).
54. A. I. Machuca-Parra, A. A. Bigger-Allen, A. V. Sanchez, A. Boutabla, J. Cardona-Vélez, D. Amarnani, M. Saint-Geniez, C. W. Siebel, L. A. Kim, P. A. D'Amore, J. F. Arboleda-Velasquez, Therapeutic antibody targeting of Notch3 signaling prevents mural cell loss in CADASIL. *J. Exp. Med.* **214**, 2271–2282 (2017).
55. E. D. Goldstein, A. Shakoor, J. J. Majersik, Branch Retinal Vein Occlusion and Venous Abnormalities in CADASIL. *Neurologist*. **25**, 178–179 (2020).
56. J. Rafalowska, A. Fidzianska, D. Dziewulska, A. Podlecka, G. M. Szpak, H. Kwiecinski, CADASIL or CADVaSIL? *Neuropathology*. **24**, 16–20 (2004).
57. M. Vanlandewijck, L. He, M. A. Mäe, J. Andrae, K. Ando, F. Del Gaudio, K. Nahar, T. Lebouvier, B. Laviña, L. Gouveia, Y. Sun, E. Raschperger, M. Räsänen, Y. Zarb, N. Mochizuki, A. Keller, U. Lendahl, C. Betsholtz, A molecular atlas of cell types and zonation in the brain vasculature. *Nat. Publ. Gr.* **0**, 1–6 (2018).
58. R. Santamaria, J. Lopez-Aguilera, R. Gonzalez De Caldas, M. Sanchez-Frias, A. Garcia-Rios, P. Buendia, P. Aljama, in *Journal of Hypertension* (2016; https://www.embase.com/search/results?subaction=viewr

ecord&id=L617793813&from=export), vol. 34.
59. V. I. H. Kwa, J. J. van der Sande, J. Stam, N. Tijmes, J. L. Vrooland, Amsterdam Vascular Medicine Group, Retinal arterial changes correlate with cerebral small-vessel disease. *Neurology*. **59**, 1536–40 (2002).
60. T. H. Rim, A. W. J. Teo, H. H. S. Yang, C. Y. Cheung, T. Y. Wong, Retinal Vascular Signs and Cerebrovascular Diseases. *J. Neuroophthalmol.* **40**, 44–59 (2020).
61. Y.-T. Ong, D. A. De Silva, C. Y. Cheung, H.-M. Chang, C. P. Chen, M. C. Wong, T. Y. Wong, M. K. Ikram, Microvascular structure and network in the retina of patients with ischemic stroke. *Stroke*. **44**, 2121–7 (2013).
62. J. J. Wang, M. L. Baker, P. J. Hand, G. J. Hankey, R. I. Lindley, E. Rochtchina, T. Y. Wong, G. Liew, P. Mitchell, Transient ischemic attack and acute ischemic stroke: associations with retinal microvascular signs. *Stroke*. **42**, 404–8 (2011).
63. F. Gekeler, K. Shinoda, M. Junger, K. U. Bartz-Schmidt, F. Gelisken, Familial Retinal Arterial Tortuosity Associated With Tortuosity in Nail Bed Capillaries Familial. *Arch. Ophthalmol.* **124**, 1492–1494 (2006).
64. G. Dougherty, M. J. Johnson, M. D. Wiers, Measurement of retinal vascular tortuosity and its application to retinal pathologies. *Med. Biol. Eng. Comput.* **48**, 87–95 (2010).
65. C. Y. L. Cheung, Y. Zheng, W. Hsu, M. L. Lee, Q. P. Lau, P. Mitchell, J. J. Wang, R. Klein, T. Y. Wong, Retinal vascular tortuosity, blood pressure, and cardiovascular risk factors. *Ophthalmology*. **118**, 812–818 (2011).
66. D. R. Seals, K. L. Jablonski, A. J. Donato, Aging and vascular endothelial function in humans. *Clin. Sci.* **120**, 357–375 (2011).
67. A. M. Reagan, X. Gu, S. Paudel, N. M. Ashpole, M. Zalles, W. E. Sonntag, Z. Ungvari, A. Csiszar, L. Otalora, W. M. Freeman, M. B. Stout, M. H. Elliott, Age-related focal loss of contractile vascular smooth muscle cells in retinal arterioles is accelerated by caveolin-1 deficiency. *Neurobiol. Aging*. **71**, 1–12 (2018).
68. C. N. Mhurchu, C. Anderson, K. Jamrozik, G. Hankey, D. Dunbabin, Hormonal Factors and Risk of Aneurysmal Subarachnoid Hemorrhage An International Population-Based, Case-Control Study Cliona. *Stroke*, 606–612 (2001).
69. A. I. Qureshi, A. A. Malik, O. Saeed, A. Defillo, G. T. Sherr, M. F. K. Suri, Hormone replacement therapy and the risk of subarachnoid hemorrhage in postmenopausal women. *J. Neurosurg.* **124**, 45–50 (2016).
70. D. Alagille, A. Estrada, M. Hadchouel, M. Gautler, M. Odièvre, J. P. Dommergues, Syndromic paucity of interlobular bile ducts (Alagille syndrome or arteriohepatic dysplasia): Review of 80 cases. *J. Pediatr.* **110**, 195–200 (1987).
71. J. C. Bucuvalas, J. A. Horn, L. Carlsson, W. F. Balistreri, S. D. Chernausek, Growth hormone insensitivity associated with elevated circulating growth hormone-binding protein in children with Alagille syndrome and short stature. *J. Clin. Endocrinol. Metab.* **76**, 1477–82 (1993).
72. J. D. Wirtschafter, Optic nerve axons and acquired alterations in the appearance of the optic disc. *Trans. Am. Ophthalmol. Soc.* **91**, 1034–1089 (1983).
73. P. Narula, J. Gifford, M. A. Steggall, C. Lloyd, I. D. M. Van Mourik, P. J. Mckiernan, H. E. Willshaw, D. Kelly, Visual Loss and Idiopathic Intracranial Hypertension in Children With Alagille Syndrome. *J. Pediatr. Gastroenterol. nu.* **43**, 348–352 (2006).
74. S. Jin, a P. Mutvei, I. V Chivukula, E. R. Andersson, D. Ramsköld, R. Sandberg, K. L. Lee, P. Kronqvist, V. Mamaeva, P. Ostling, J.-P. Mpindi, O. Kallioniemi, I. Screpanti, L. Poellinger, C. Sahlgren, U. Lendahl, Non-canonical Notch signaling activates IL-6/JAK/STAT signaling in breast tumor cells and is controlled by p53 and IKKα/IKKβ. *Oncogene*. **32**, 4892–902 (2013).
75. G. Matsuura, Y. Higashimoto, J. Iwai, K. Murayama, H. Horie, T. Suzuki, A case of Alagille syndrome with hepatic-duct obliteration presenting intracranial hemorrhage. *Chiba Med. J.* **89**, 181–185 (2013).
76. J. A. Cowan, G. Barkhoudarian, L. J. S. Yang, B. G. Thompson, Progression of a posterior communicating artery infundibulum into an aneurysm in a patient with Alagille syndrome. Case report. *J. Neurosurg.* **101**, 694–6 (2004).
77. E. B. A. Vorstman, P. Anslow, D. M. Keeling, G. Haythornthwaite, H. Bilolikar, M. T. McShane, Brain haemorrhage in five infants with coagulopathy. *Arch. Dis. Child.* **88**, 1119–1121 (2003).
78. S. Agrawal, V. Chennuri, P. Agrawal, Genetic Diagnosis in an Indian Child with Alagille Syndrome. *Indian J. Pediatr.* **82**, 653–654 (2015).
79. A. Rachmel, A. Zeharia, M. Neuman-Levin, R. Weitz, R. Shamir, G. Dinari, Alagille syndrome associated with Moyamoya disease. *Am. J. Med. Genet.* **33**, 89–91 (1989).
80. L. C. Baird, E. R. Smith, R. Ichord, D. A. Piccoli, T. J. Bernard, N. B. Spinner, R. M. Scott, B. M. Kamath, Moyamoya syndrome associated with Alagille syndrome: outcome after surgical revascularization. *J Pediatr*. **166**, 470–473 (2015).
81. D. O'Connell, C. Kaliaperumal, N. Fanning, G. Wyse, G. Kaar, Superior cerebellar aneurysm causing subarachnoid haemorrhage in a 17-year-old with alagille syndrome. *Br. J. Neurosurg.* **26**, 287–289 (2012).
82. J. Fiorda-Diaz, M. Shabsigh, G. Dimitrova, S. Soghomonyan, G. Sandhu, Perioperative Management of Subarachnoid Hemorrhage in a Patient with Alagille Syndrome and Unrepaired Tetralogy of Fallot: Case Report. *Front. Surg.* **4**, 72 (2017).
83. L. M. Tumialán, S. S. Dhall, P. R. Tomak, D. L. Barrow, Alagille Syndrome and Aneurysmal Subarachnoid Hemorrhage. *Pediatr. Neurosurg.* **42**, 57–61 (2006).
84. F. Frongillo, G. Bianco, N. Silvestrini, M. C. Lirosi, A. M. Sanchez, E. Nure, R. Gaspari, A. W. Avolio, G. Sganga, S. Agnes, Acute Liver Failure in an Adult, a Rare Complication of Alagille Syndrome: Case Report and Brief Review. *Transplant. Proc.* **47**, 2179–2181 (2015).
85. R. C. Gaba, R. P. Shah, A. A. Muskovitz, G. Guzman, E. A. Michals, Synchronous moyamoya syndrome and ruptured cerebral aneurysm in Alagille syndrome. *J. Clin. Neurosci.* **15**, 1395–8 (2008).
86. H.-G. Schlosser, T. Kerner, C. Woiciechowsky, G. Benndorf, Multiple cerebral aneurysms and subarachnoid hemorrhage in a patient with Alagille syndrome. *AJNR Am. J. Neuroradiol.* **25**, 1366–1367 (2004).

## Acknowledgments:

We thank Bettina Semsch for help with tail vein injections. We thank Soniya Savant for her input regarding vascular phenotypes and single cell sequencing library preparation (not included in manuscript). We thank Katarina Tiklova for her advice and help with single cell sequencing library preparation and FACS sorting (not included in manuscript). We thank Liqun He

and Christer Betsholtz for their help with single cell analysis (not included in manuscript). Further, we thank Tomasz Krzywkowski and Mats Nilsson for their efforts to help us adapt retina padlock probe in situ hybridization to retina (not included in manuscript). We thank the Rickard Sandberg group especially Gösta Winberg for providing us with Tn5 enzyme and other buffers for SmartSeq2 libraries and their input on the library quality (not included in manuscript). We thank SciLife for their help with single cell RNA sequencing and bioinformatic analysis (not included in manuscript). We thank Jianshe Wang and Liting Li (University of Fudan) for discussions and analysis of patient data, not included in this manuscript. The monoclonal antibody NF-RT97 developed by Wood, J. obtained from the Developmental Studies Hybridoma Bank, created by the NICHD of the NIH and maintained at The University of Iowa, Department of Biology, Iowa City, IA 52242.

**Funding:**

Center of Innovative Medicine (CIMED) Grant (2-538/2014-29) (ERA)

Ragnar Söderberg Foundation (Swedish Foundations' Starting Grant, S11/20) (ERA)

Swedish Research Council (2019-01350) (ERA)

EASL Daniel Alagille Award (ERA)

Heart and Lung Foundation (20170723) ERA

KI Funding (2-2110/2019-7, 2-560/2015-280) ERA

Alex and Eva Wallström Foundation (ERA)

Wera Ekströms Stiftelse (SH)

"KI-MU" program co-financed from European Social Fund and the state budget of the Czech Republic (CZ.1.07/2.3.00/20.0180) (VB)

Czech Science Foundation project Expro (GX19-28347X) (VB)

CzechNanoLab Research Infrastructure supported by MEYS CR (LM2018110) (JK)

**Competing interests:** The authors declare that they have no competing interests. One project in ERA lab is funded by modeRNA, unrelated to this manuscript (no personal remuneration). UL holds a research grant from Merck Healthcare KGaA, but no personal remuneration, unrelated to this manuscript.

**Author contributions:**

Conceptualization: SH, ERA, TZ, JK

Methodology: SH, JL, BRJ, MH

Investigation: SH, NVH, JL, NH, EV, MK, JS, MS, AJ, BF, ERA

Formal analysis: SH, NVH, KM, MK, JS; JL, EV, NH, ERA

Visualization: SH, JL, NH, EV, BRJ, ERA

Supervision: TZ, JK, ERA

Funding acquisition: SH, VB, UL, JK, ERA

Resources: LTF, FA, KTF, BF, ERA

Writing—original draft: SH, ERA

Writing—review & editing: SH, NVH, JL, MK, LTF, VB, UL, FA, KTF, BF, ERA

Data and materials availability:

All data are available in the main text, figures, tables, or the supplementary data.

Table 1. **Overview of patients with Alagile syndrome reported with vascular abnormality.** Summary of patients identified in Systematic Review, with ALGS and intracranial bleeding, including type of bleed, cause or associated insult, and sex data. These data are the basis of Fig 1B.

| Sex | Age (years) | IC event | Coagulation & bilirubin data | Provoked (coagulopathy / trauma) or Idiopathic | Ref | Patient # (as in Table S1) |
|---|---|---|---|---|---|---|
| Males | Neonatal | Subdural hematoma after birth trauma. (Patient #10) | NR. | Minor trauma | (*26*) | 107 |
| | 61 days | Intracranial hemorrhage.<br>Recovered. | Ascribed to Vitamin K deficiency (cholestatic coagulopathy) | Coagulopathy | (*75*) | 131 |
| | 22 months | Epidural hematoma, and parenchymal and intraventricular bleeds, after falling from a chair. | Normal coagulation factors | Minor trauma | (*7*) | 124 |
| | 2 | Epidural hematoma after minor accidental head trauma.<br>Fatal. | NR | Minor trauma | (*6*) | 120 |
| | 2.3 | Large epidural hematoma due to minor head trauma.<br>Paper-thin cranial bones. | NR | Minor trauma | (*6*) | 121 |
| | 6 | Intracranial bleed after liver transplant.<br>Fatal.<br>(Patient #19 in Emerick et al 2005) | Mild disseminated intravascular coagulation. | Coagulopathy | (*2*, *26*) | 108 |
| | 12 | Hematoma at age 12 with right parietal fracture but no history of trauma.<br>Stroke at age 18. | NR | Probably minor trauma | (*4*) | 139 |
| | 13 | Subarachnoid hemorrhage. | NR | Idiopathic | (*58*) | 152 |

| | | | | | | |
|---|---|---|---|---|---|---|
| | 23 | Two events:<br>First event: ruptured basilar tip aneurysm.<br>Second event unclear: red blood cells in cerebrospinal fluid. Aneurysm of posterior communicating artery present but no evidence of rupture.<br>Aneurysm clipped and patient recovered. | At second event:<br>16.1s Prothrombin<br>40.6s partial thrompboplastin<br>Total bilirubin 8.6mg/dL | Coagulopathy | (*76*) | 106 |
| Females | 10 weeks | Subdural hematoma, posterior fossa and around tentorium. | Raised prothrombin time.<br>Raised activated partial prothrombin time.<br>Thrombin and fibrinogen normal.<br>Conjugated hyperbilirubinaemia | Coagulopathy | (*77*) | 69 |
| | 5 months | Intracerebral hemorrhage.<br>Fatal.<br>Multiple large, thin-walled vessels at autopsy. | Hemoglobin 5.9 g/dl.<br>Prothombin time 20 s (control of 15),<br>Total bilirubin 8.8 mg/dl,<br>direct 5.2 mg/dl, | Coagulopathy | (*78*) | 7 |
| | 22 months | Evidence of old intracerebral hemorrhage on CT scan. | NR for time of hemorrhage | Idiopathic | (*79*) | 49 |
| | 2 | Intracerebral hemorrhage.<br>Fatal.<br>Multiple large, thin-walled vessels at autopsy. | Normal coagulation values. | Idiopathic | (*6*) | 34 |
| | 4 | Epidural hematoma after a fall (40cm).<br>Fatal.<br>At autopsy: thinning of arterial walls with apoptotic muscle cell layer and thin cranial bones. | NR. | Minor trauma | (*8*) | 46 |

| | | | | | | |
|---|---|---|---|---|---|---|
| | 4 | MCA territory stroke and right frontal stroke after cardiac procedure.<br>Moyamoya syndrome.<br>EDAS (encephaloduroarteriosynangiosis) for revascularization.<br>Fatal left thalamic hemorrhage two years after EDAS.<br>(Patient #5 in article) | NR | Idiopathic | (*80*) | 11 |
| | 9 | Subarachnoid hemorrhage after minor head trauma.<br>(Patient #2 in article) | NR. | Minor trauma | (*26*) | 20 |
| | 17 | Subarachnoid hemorrhage from superior cerebellar artery aneurysm.<br>Aneurysms coiled and patient recovered. | "laboratory testing was insignificant other than urea of 8.2 and deranged liver function tests (…)" | Idiopathic | (*81*) | 44 |
| | 17 | Two events:<br>First event: intracranial epidural hematoma.<br>Second event: Subarachnoid hemorrhage from communicating artery aneurysm.<br>Recovered. | "Laboratory tests were unremarkable" | Idiopathic | (*82*) | 28 |
| | 20 | Intracranial hemorrhage due to ruptured middle cerebral artery aneurysm. (Patient #5) Fatal. | NR | Idiopathic | (*26*) | 21 |
| | 21 | Catastrophic subarachnoid hemorrhage and intraparenchymal hematoma.<br>Possible basilar artery aneurysm rupture.<br>Fatal. | NR | Idiopathic | (*83*) | 65 |
| | 25 | Subarachnoid hemorrhage from large saccular ruptured terminal basilar artery aneurysm. Fatal. | NR. Autopsy | Idiopathic | (*37*) | 18 |

| | | | | | | |
|---|---|---|---|---|---|---|
| | 28 | Cerebral and ocular hemorrhage.<br>Urgent orthotopic liver transplant, recovered. | INR 3.18<br>Hemoglobin 5.9 g/dL<br>Platelets 90,000/$mm^3$<br>Total bilirubin 63 mg/dL | Coagulopathy | (*84*) | 30 |
| | 28 | Subarachnoid hemorrhage from vertebrobasilar junction aneurysm. Stent exclusion of aneurysm, patient recovered. | Total bilirubin 1.3 mg/dL<br>Alkaline phosphatase 444 units/L [normal 40–125 units/L] | Idiopathic | (*85*) | 31 |
| | 30 | Subarachnoid hemorrhage due to a ruptured 8-mm aneurysm of the right supraclinoid internal carotid artery.<br>Right parietal subdural hematoma.<br>Surgical clipping of aneurysm, patient recovered. | NR | Idiopathic | (*86*) | 59 |

Table 2. **Vascular events in patients with Alagille syndrome and biliary atresia.** Vascular anomalies quantified in the retinographs in Figure 8. (*) labels the age and vascular anomaly for which the blood values are provided. ALGS, Alagille syndrome; BA, biliary atresia; m, month.

| ID | Diagnosis | Sex | Age eye exam (y) | Bilirubin total/ conjugated (μM/L) | Bile acids (μM/L) | INR | Platelet count ($10^9$/L) | Vascular event (age of event, * denotes age for which blood analysis at right is described) | Bilirubin total/ conjugated (μM/L) | Bile acids (μM/L) | INR | Platelet count ($10^9$/L) | Follow up until (y) |
|---|---|---|---|---|---|---|---|---|---|---|---|---|---|
| | reference value | | | 16/4 | < 7 | < 1.2 | 200-400 | | 16/4 | < 7 | < 1.2 | 200-400 | |
| a | ALGS | F | 9 | 76/58 | 239 | 1.21 | 141 | Surgery-related hemorrhage (10*), nosebleed (15), GI bleed (Grade 1 at 10, Grade 4 at 17), splenic infarction (18) | 58/39 | 239 | 1.38 | 117 | 18 |
| b | ALGS | F | 10 | 6/1 | 11 | 1.02 | 281 | Nosebleed (10*) | 6/1 | 11 | 1.02 | 281 | 18 |
| c | ALGS | F | 12 | 9/2 | 25 | 1 | 267 | N/A | | | | | 18 |
| d | ALGS | F | 2 | 6/<2 | 3 | 1 | 486 | N/A | | | | | 6 |
| e | ALGS | F | 5 | 4/<2 | 3 | 1 | 295 | N/A | | | | | 13 |
| f | ALGS | M | 4 | 5/<2 | 3 | 1 | 334 | Coagulopathy-related bleed (1m*) | 62/37 | 79 | >8 | 417 | 4 |
| | BA | F | 8 | 24/8 | 285 | 1.14 | 65 | Bruising (9*), esophageal varices (10) | 32/16 | 312 | 1.17 | 60 | 18 |
| | BA | M | 15 | N/A | N/A | N/A | N/A | N/A | N/A | N/A | N/A | N/A | 18 |
| | BA | F | 11 | 8/1 | 4 | 0.99 | 141 | Nosebleed, GI bleeding, bruising (all three events at age 14* and 15) | 6/1 | | 0.9 | 222 | 18 |
| | BA | F | 10 | 11/3 | | 1.2 | 67 | GI bleeding (7*) | 5/1 | | 1.16 | 58 | 18 |